GENUINE MULTIPATH INTERFERENCE

ZHAO ZHUO

SCHOOL OF PHYSICAL AND MATHEMATICAL SCIENCES

2020

GENUINE MULTIPATH INTERFERENCE

ZHAO ZHUO

SCHOOL OF PHYSICAL AND MATHEMATICAL SCIENCES

A thesis submitted to the Nanyang Technological University in partial
fulfilment of the requirement for the degree of Doctor of Philosophy

2020

Statement of Originality

I hereby certify that the work embodied in this thesis is the result of original research done by me except where otherwise stated in this thesis. The thesis work has not been submitted for a degree or professional qualification to any other university or institution. I declare that this thesis is written by myself and is free of plagiarism and of sufficient grammatical clarity to be examined. I confirm that the investigations were conducted in accord with the ethics policies and integrity standards of Nanyang Technological University and the research data are presented honestly and without prejudice.
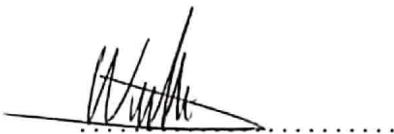
24 August 2020

. . . .

Zhao Zhuo   Date

Supervisor Declaration Statement

I have reviewed the content and presentation style of this thesis and declare it of sufficient grammatical clarity to be examined. To the best of my knowledge, the thesis is free of plagiarism and the research and writing are those of the candidate's except as acknowledged in the Author Attribution Statement. I confirm that the investigations were conducted in accord with the ethics policies and integrity standards of Nanyang Technological University and that the research data are presented honestly and without prejudice.

Assoc. Prof.
David Wilkowski

21/01/2020

Date

Authorship Attribution Statement

This thesis contains material from paper published in the following peer-reviewed journal in which I am listed as an author.

"Paradoxical consequences of multipath coherence: Perfect interaction-free measurements", Phys. Rev. A 98, 022108

The contributions of the co-authors are as follows:

1. Profs. Laskowski and Paterek provided project direction, and assisted in the proofs.

2. Prof. Dakić provided information on the density cube model.

3. Prof. Rutkowski provided idea of the proof in the Appendix.

4. Dr. Markiewicz provided discussion on interaction-free measurements in alternatives to quantum mechanics.

5. Mr. Mondal worked on the cubes model.

6. I provided parts of the trade-off proof, orthogonality equations proof and consistency proof, explicit examples within the cubes model, discussion of applications of higher-order interference and prepared versions of the manuscript.

....   24 August 2020
                                           ....
Zhao Zhuo   Date

Authorship Attribution Statement
(continued)

This thesis contains material from paper published in the following peer-reviewed journal in which I am listed as an author.

"An atomic test of higher-order interference", Phys. Rev. A 101, 052111

The contributions of the co-authors are as follows:

1. Profs. Couteau, Wilkowski and Paterek provided project direction and assisted in calculations.

2. Prof. Wilkowski was consulted for experimental details.

3. Mr. Lee contributed to the proofs of robustness of Sorkin's quantity in the atomic system, calculations of the tritter and all the blockers.

4. I contributed to calculations of the tritter, blocking via spontaneous emission, interference fringes and noise and error analysis.

....   24 August 2020
                                              ....
Zhao Zhuo   Date

Abstract

Quantum mechanics predicts that for single quanta interference is limited to pairs of events. It can therefore be categorized as "second-order interference theory". In this thesis, we wish to explore possibility of "higher-order interference", exemplified by generalizations of Young's double slit experiment to three and more paths. We show in the thesis that it is possible to create higher-order interference using non-linear processes within second quantization formalism and it is present in some extensions of quantum mechanics. We also discuss operational advantages of utilizing higher-order interference and propose precise experiment with atoms to bound its presence.

Acknowledgement

Contents

List of Symbols

ψ	Wavefunction
$\langle\psi\|$	Bra
$\|\psi\rangle$	Ket
$\mathbb{1}$	Identity matrix
$\mathbf{0}$	Zero matrix
Tr	Trace
∇^2	Laplacian operator
a	Annihilation operator
$a^\dagger$	Creation operator
I	Intensity
α	Coherent state
$\mathcal{S}^n$	Sorkin's quantity of nth order
$\mathbb{E}$	Expectation value
Var	Variance
P_{ijk}	Probability of detection with paths i, j, k open
$\bar{}$	Interaction picture
$\hat{}$	Schrödinger picture
$\tilde{}$	Renormalized state

Chapter 1

Introduction

This thesis aims to explore "genuine multipath interference". First we will introduce the familiar concept of "interference", and then define the phrase "genuine multipath". We begin with interference of classical objects, followed by quantum interference, abstract definition of higher-order interference and present evidences and scenarios showing absence of higher-order interference in experiments.

1.1 Interference

Interference is a physical phenomenon where two or more waves meet at the same point. The waves have to be of the same type, e.g. waves on water, electromagnetic waves in classical domain or "probability waves" in quantum domain.

1.1.1 Classical interference

In classical interference, the displacement of the resulting wave is equal to the sum of the displacements of the individual waves at the point.

$$A_R = A_1 + A_2 \tag{1.1}$$

where A_j denotes the displacement of the constituent waves and A_R that of the resulting wave. Therefore, in the simplest case of plane waves with fixed wavelengths, complete constructive and destructive interference occurs if their relative phase difference is 0 and π respectively (up to addition of integer multiple of 2π).

1.1.2 Evidence of classical interference

One example of classical interference is double-slit experiment, e.g. with water waves or electromagnetic waves, see Fig. 1.1. Another example is noise cancellation, in which a speaker produces an equal but out-of-phase sound wave in order to destructively interfere with surrounding noise.

Figure 1.1: Interference of water waves created by bouncing two spheres simultaneously. The result is alternating regions of destructive interference, with calm water surface, and regions of constructive interference, with large ripples. Image adapted from Youtube channel "Veritasium" [1].

1.1.3 Quantum interference

In abstract formulation, quantum interference can be observed in the transition from one state to another. Quantum states can be described in bra-ket notation as:

$$
\begin{aligned}
|\psi\rangle &= \sum_i |i\rangle \langle i|\psi\rangle \\
&= \sum_i \psi_i |i\rangle
\end{aligned}
\tag{1.2}
$$

where $|i\rangle$ are the vectors forming a basis, ψ_i are complex numbers satisfying normalization condition $\sum_i |\psi_i|^2 = 1$. If we want to calculate the transition

probability from $|\psi\rangle$ to $|\phi\rangle$, the usual approach is to take the inner product:

$$
\begin{aligned}
P(|\psi\rangle \longrightarrow |\phi\rangle) &= |\langle\psi|\phi\rangle|^2 \\
&= \sum_{i,j} \langle\psi|i\rangle \langle i|\phi\rangle \langle\phi|j\rangle \langle j|\psi\rangle \\
&= \sum_{i,j} \psi_i^* \phi_i \phi_j^* \psi_j \\
&= \sum_{i=j} |\psi_i|^2 |\phi_i|^2 + \sum_{i\neq j} \psi_i^* \phi_i \phi_j^* \psi_j
\end{aligned}
\tag{1.3}
$$

If the quantum particle were prepared in state $|\psi\rangle = |i\rangle$, the transition probability would be $|\phi_i|^2$. It is the presence of the second term in the expression that reveals the superposition of different $|i\rangle$s in $|\psi\rangle$. This term is called "quantum interference term". It is important to note that quantum interference happens for each individual quantum particle, i.e. a quantum particle can interfere with itself.

1.1.4 Evidence of quantum interference

When Einstein explained the photoelectric effect, the wave-particle dual nature of light became apparent. De Broglie hypothesised that similar effects should be present with massive particles too. Indeed their interference has been experimentally verified for electrons [2], fullerenes [3,4] and even larger molecules [5]. Futhermore, quantum interference is required to explain single-click version of the double slit experiment [6].

1.1.5 Higher-order interference

Consider now an interference experiment with three or more slits. It turns out that in quantum mechanics, the probability to find an object around a given point on the screen is a simple arithmetic sum of the probabilities obtained with double slit experiments. This is in contrast to the double-slit experiment per se, where we cannot express the fringe pattern as the sum of the single-slit patterns.
We now introduce the term "order of interference". Consider the experiments with slits, the first order of interference is equal to the intensity on the screen when one slit is open.

$$
\mathcal{S}^1 \equiv I_1^1
\tag{1.4}
$$

where I is the photon intensity (particle count for electron experiment) formed on the screen at any fixed point with a particular experimental arrangement. Superscript denotes the total number of slits, subscript denotes the indices of slits open. The second order interference, which is known to be non-zero from the experimental results on quantum particles is defined as:

$$\mathcal{S}^2 \equiv I_{12}^2 - I_1^1 - I_2^1 \tag{1.5}$$

Similarly, for three slits [7]:

$$\mathcal{S}^3 \equiv I_{123}^3 - I_{12}^2 - I_{13}^2 - I_{23}^2 + I_1^1 + I_2^1 + I_3^1 \tag{1.6}$$

"Genuine multipath interference" is then defined as third- and higher-order interference effects which cannot be reduced to sum of lower-order interferences, which in our notation above is signified by $\mathcal{S}^3 \neq 0$.

1.1.6 Sorkin's quantity

The "hierarchy of order of interference" in this thesis was introduced by Rafael Sorkin [7] to generalize interference effects. Intensity in our case is generalized to a non-negative number associated to a set, which he calls its "quantum measure". The nth order of interference is:

$$\mathcal{S}^n \equiv I_{123...n}^n - \sum I_{123...(n-1)}^{n-1} + \sum I_{123...(n-2)}^{n-2} \cdots + (-1)^{n-1} \sum_k^n I_k^1 \tag{1.7}$$

where the sum runs over all combinations of distinct "sets" (or slits in our case) and the sign alternates between each summand.

These expressions can be recursively obtained using the following lemma [7]:

Lemma 1.

$$\mathcal{S}^{n+1}(1, 2, 3 \cdots n, x) = \mathcal{S}^n(1 \cup x, 2, 3 \cdots n) - \mathcal{S}^n(x, 2, 3 \cdots n) - \mathcal{S}^n(1, 2, 3 \cdots n)$$

An immediate consequence is that $\mathcal{S}^{n+1}$ vanishes if $\mathcal{S}^n$ is linear in its arguments. For example,

$$\mathcal{S}^2 = I_{12}^2 - I_1^1 + I_2^1 \tag{1.8a}$$
$$\text{if} \quad I_{12}^2 = I_1^1 + I_2^1 \tag{1.8b}$$
$$\text{then} \quad \mathcal{S}^2 = 0 \tag{1.8c}$$

Second consequence is that if $\mathcal{S}^n$ is identically 0, so will $\mathcal{S}^{n+k}$, where $k > 0$. A particular physical theory can then be categorized by the last order at

which the Sorkin's quantity is non-zero. If we set the first order $\mathcal{S}^1 = 0$, it means no measurement amplitude is possible, hence zero-th level theories are trivial and uninteresting. The second order expresses the additivity of classic measure theory, where probabilities from distinct events, with classical particles, simply add together. Quantum mechanics violates this classical additivity, and it is an example of a model in the class of "second-order measure theory". Sorkin showed that $\mathcal{S}^3 = 0$ for a quantum model with individual quanta and we will repeat this argument later in this thesis.

1.1.7   Link between Sorkin's quantity and Born's rule

The observation that quantum mechanics does not give rise to multipath interference was made for the first time about 20 years ago [7], and was linked to the validity of Born's rule.
If we define the intensities as:

$$I_{12}^2 \sim |\psi_1 + \psi_2|^2 \tag{1.9}$$

$$I_1^1 \sim |\psi_1|^2 \tag{1.10}$$

$$I_2^1 \sim |\psi_2|^2 \tag{1.11}$$

then $\mathcal{S}^3 = 0$ by:

$$\begin{aligned}
\mathcal{S}^3 = {} & |\psi_1 + \psi_2 + \psi_3|^2 \\
& - |\psi_1 + \psi_2|^2 - |\psi_1 + \psi_3|^2 - |\psi_2 + \psi_3|^2 \\
& + |\psi_1|^2 + |\psi_2|^2 + |\psi_3|^2
\end{aligned} \tag{1.12}$$

since the intensity at any point on the screen is proportional to the square of the sum of the probability amplitudes, only products of two amplitudes are present in interference terms. So naturally higher-order interference is missing. Experiments were set up to look for genuine multipath interference and to test the Born rule [8–11] and found absence of higher-order interference.

1.1.8   Observed absence of higher-order interference

We can experimentally determine if third-order interference pattern is indeed zero in nature. Some experiments were done with single photons [8–10] and in a NMR setup [11] and show that indeed there is a strict upper-bound on higher-order interference compared to the second-order interference.
In slit experiments where exotic non-classical looped trajectories are considered [12], the quantum interference effects can be observed too, and give rise to $\mathcal{S}^3 \neq 0$, but only in the near-field region.

1.1.9 Operational advantage of higher-order interference

In addition to being of fundamental interest, higher-order interference also has practical implications. It has been shown that multipath interference provides an advantage over quantum mechanics in the task called the "three collision problem" [13] and may be advantageous over quantum algorithms [14], although this is not the case in searching [15]. It will be demonstrated later in the thesis that higher-order interference improves on the efficiency of "interaction-free measurements" over quantum mechanics.

1.2 Plan of the thesis

Having described basic motivations to look at higher-order interference, we proceed to the main body of the thesis, which is organized as follows.

Chapter 2 presents the theory for an atomic equivalent of optical triple-slit experiment. We wish to test the universality of quantum mechanical framework, since it is expected to hold not only in optical experiments, but in all physical systems. The bound on Sorkin's quantity may be lowered from 10^{-4} in earlier optical experiments to 10^{-5} in our proposed atomic setup, due to the increased number of particles and the number of experiments that can be done within relatively short time.

Chapter 3 explores the possibility of non-zero Sorkin's quantity within canonical quantum mechanics. The idea is to consider interference effects within second quantization. It turns out that Sorkin's quantity can be used to detect non-linear elements in experimental setups. The corresponding verification is currently under way, using quantum optics.

Chapter 4 introduces a "post-quantum" theory of "density cube", extending the concept of quantum coherence to three levels, and explores the consequences and possible advantages of the model when compared to the quantum model. We argue that the obtained advantage is too strong to be present in nature. This sheds light on why we might never be able to observe higher-order interference with singe quanta theoretically.

Chapter 2

Interference of atoms: analogue of three-slit experiment [1]

The double-slit experiment with single particle at a time is a landmark of quantum phenomena. This observation has been linked to the validity of Born's rule and it was first tested in three-slit experiments with single photons [8,9], and mimicked with nuclear magnetic resonance (NMR) [10]. The figure of merit measured in these experiments is the magnitude of the triple-slit interference term (that is supposed to be vanishing) as compared to the magnitude of the double-slit fringes. This ratio was measured down to the level of 10^{-2} in [8] and in the recent optics experiment it was improved to 10^{-4} [11] in semi-classical regime, beating the precision of the NMR experiment [10], which is 10^{-3}. We propose to test higher-order interference using atomic system. The main motivation is to test Born's rule, where it is expected to be universally valid and yet it has not been verified with atoms.

2.1 Advantages of atomic experiment

It is important to mention that small non-zero third-order interference term is expected in optical multi-slit experiments, but is measurable only in near field regime. In essence, it is due to different boundary conditions in the experiments with many open slits versus superposition of waves emerging from many single slits [16–19]. These effects have been recently observed in [12, 20]. Moving away from the spatial domain removes the issue with the boundary conditions. In particular, in our proposal the spatial superposition is replaced by superposition of energy eigenstates. Furthermore, in contradistinction to the NMR setup, atoms can be prepared in essentially

---

[1]Based on Phys. Rev. A 101, 052111

pure states whereas NMR sample is in a highly mixed state

$$\rho_{NMR} = (1 - \varepsilon)\frac{\mathbb{1}}{d} + \varepsilon\rho_{pure}$$

where ε is of order 10^{-5} or less [21,22]. In other words, if the complete initial NMR state was taken into account there would be almost no interference to start with. Finally, and different from Ref. [10], we aim at providing complete analogue of the spatial experiment which includes models of blocking the slits within the atomic system. Ultimately, due to parallel processing with many atoms, the atomic setup can also improve one order of magnitude the results on the figure of merit from the previous experiments.

2.2   Experimental proposal
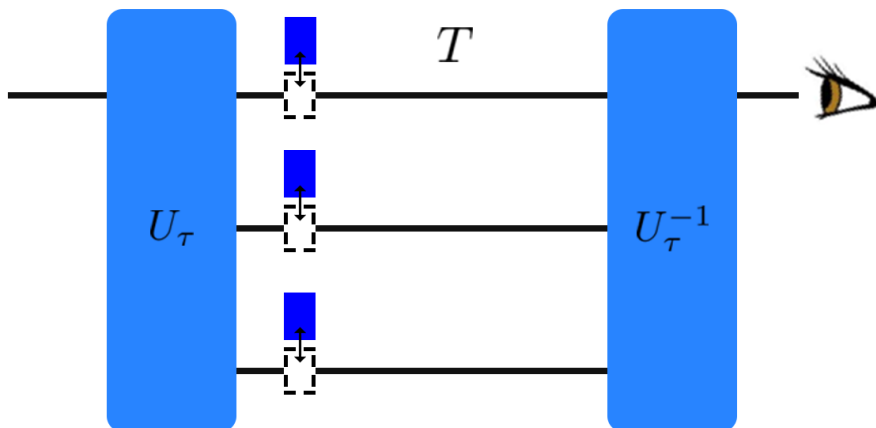
Figure 2.1: Schematic of the experiment testing third-order interference. Temporal order is from left to right. A particle is prepared in one of the three states and enters the tritter box U_τ that prepares a superposition over the three possibilities. The boxes inside the interferometer denote the "blockers", i.e. they eliminate particles in states that are being blocked. The blockers can be put in or removed from the setup at will. The particle evolves inside the interferometer for time T. The second tritter U_τ^{-1} closes the interferometer loop after which the probability of registering the particle in the initial state is estimated. In order to find κ, see Eq. 2.1, one repeats this experiment for all combinations of placing blockers in the setup.

A generic experiment testing third-order interference is depicted and described in Fig. 2.1. In the spatial domain it is a version of Mach-Zehnder

interferometer with three paths and path blockers inside the interferometer. In the atomic setup we propose to replace the spatial paths with energy eigenstates. The input state is then a ground state of the atom. The role of the tritter, generalisation of the beam-splitter to three paths [23], is to prepare suitable coherent superposition of the energy states and we shall explain how this can be achieved with generalised Raman transitions in Subsec. 2.2.2. The effect of the blockers is to proceed with the experiment only if the atoms are not in the blocked state, without affecting coherence between the remaining states. This is reminiscent to Leggett's "ideal negative result" procedures [24,25]. We shall describe various ways of realising blockers within the atomic system. The final stage of the setup comprises one more tritter and measurement of the probability that the atom is in the initial ground state. Altogether the atomic setup is a Ramsey interferometer, with three energy eigenstates. We introduce the figure of merit κ here, defined as the ratio of the hypothetical third-order interference to the sum of the expected second-order interference,

$$\kappa = \frac{\mathcal{S}^3}{|\mathcal{S}^2_{12}| + |\mathcal{S}^2_{13}| + |\mathcal{S}^2_{23}|} \qquad (2.1)$$

where $\mathcal{S}^2_{jk}$ is the second-order Sorkin's quantity with slits j, k open. This figure of merit allows us to gauge the strength of the unknown third-order interference against the known second-order interference.

2.2.1 Initial state

We envisage this experiment with atoms such as Strontium which in suitable energy subspace have the tripod energy diagram given in Fig. 2.2. The three lower states are stable and we shall refer to them as ground states. We assume they have different magnetic quantum number and hence can be addressed individually with suitably polarised and arranged lasers. We take the atoms inside external magnetic field and hence the three states have depicted energy differences. This energy configuration gives rise to a natural input state to the setup in Fig. 2.1, i.e. $|1\rangle$. We note that the initial state is practically pure after optical pumping and if needed states $|2\rangle$ and $|3\rangle$ can be obtained in essentially noiseless way via stimulated Raman adiabatic passage [26].

2.2.2 Tritter

Here, we explain how to realize superposition over the three ground states. Let us first consider only the $|2\rangle \leftrightarrow |e\rangle$ transition. This two-level system can
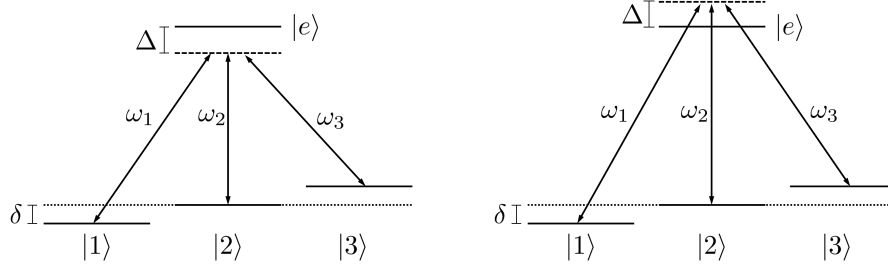
Figure 2.2: Energy diagram for (a) tritter and (b) inverse tritter using the sign change of detuning Δ.

be described by Rabi oscillation. The total Hamiltonian $\hat{H}$ of the subsystem is separated into two components, the bare Hamiltonian $\hat{H}_0$, and the driving field Hamiltonian $\hat{H}_{int}$:

$$\hat{H} = \hat{H}_0 + \hat{H}_{int} \tag{2.2a}$$

$$\hat{H}_0 = \hbar \begin{bmatrix} 0 & 0 \\ 0 & \omega_2 + \Delta \end{bmatrix} \tag{2.2b}$$

$$\hat{H}_{int} = \hbar \begin{bmatrix} 0 & \Omega \cos(\omega_2 t) \\ \Omega^* \cos(\omega_2 t) & 0 \end{bmatrix} \tag{2.2c}$$

where $\omega_2 + \Delta$ is the frequency of the transition, Δ the detuning, ω_2 is laser frequency, and we chose the energy of the ground state $|2\rangle$ to be 0.

We turn to interaction picture to simplify the Hamiltonian further. The transformation is as follows:

$$\hat{H}_B = \hbar \begin{bmatrix} 0 & 0 \\ 0 & \omega_2 \end{bmatrix} \tag{2.3}$$

$$
\begin{aligned}
\bar{H}_{int} &= e^{i\hat{H}_B t/\hbar} \left(\hat{H} - \hat{H}_B \right) e^{-i\hat{H}_B t/\hbar} \\
&= \hbar \begin{bmatrix} 1 & 0 \\ 0 & e^{i\omega_2 t} \end{bmatrix} \begin{bmatrix} 0 & \Omega \cos(\omega_2 t) \\ \Omega^* \cos(\omega_2 t) & \Delta \end{bmatrix} \begin{bmatrix} 1 & 0 \\ 0 & e^{-i\omega_2 t} \end{bmatrix} \\
&= \frac{\hbar}{2} \begin{bmatrix} 0 & \Omega(1 + e^{-2i\omega_2 t}) \\ \Omega^*(1 + e^{2i\omega_2 t}) & 2\Delta \end{bmatrix}
\end{aligned}
\tag{2.4}
$$

We make the Rotating Wave Approximation and simplifies the interaction Hamiltonian as:

$$\bar{H}_0 = \hbar \begin{bmatrix} 0 & 0 \\ 0 & \omega_2 \end{bmatrix} \tag{2.5a}$$

$$\bar{H}_{int} = \frac{\hbar}{2} \begin{bmatrix} 0 & \Omega \\ \Omega^* & 2\Delta \end{bmatrix} \tag{2.5b}$$

13

Similarly, for the three ground levels, the total Hamiltonian is

$$
\hat{H} = \begin{bmatrix}
0 & 0 & 0 & \Omega_1 \cos(\omega_1 t) \\
0 & \delta & 0 & \Omega_2 \cos(\omega_2 t) \\
0 & 0 & 2\delta & \Omega_3 \cos(\omega_3 t) \\
\Omega_1 \cos(\omega_1 t) & \Omega_2 \cos(\omega_2 t) & \Omega_3 \cos(\omega_3 t) & \omega_1 + \Delta
\end{bmatrix}
\qquad (2.6)
$$

We move to the interaction picture with the base Hamiltonian

$$
\hat{H}_B = \begin{bmatrix}
0 & 0 & 0 & 0 \\
0 & \delta & 0 & 0 \\
0 & 0 & 2\delta & 0 \\
0 & 0 & 0 & \omega_1
\end{bmatrix}
\qquad (2.7)
$$

In this picture, the perturbation Hamiltonian reads:

$$
\bar{H}_{int} = \frac{\hbar}{2} \begin{bmatrix}
0 & 0 & 0 & \Omega \\
0 & 0 & 0 & \Omega \\
0 & 0 & 0 & \Omega \\
\Omega & \Omega & \Omega & 2\Delta
\end{bmatrix}
\qquad (2.8)
$$

where we used rotating wave approximation and simplify all three Rabi frequencies Ω_j are real and equal to Ω. The corresponding Schrödinger equations are:

$$
\dot{\bar{c}}_j = \frac{-i\Omega}{2} \bar{c}_e \quad \text{for} \quad j = 1, 2, 3
\qquad (2.9)
$$

$$
\dot{\bar{c}}_e = \frac{-i\Omega}{2} \left(\sum_j^3 \bar{c}_j + \Delta \bar{c}_e \right)
\qquad (2.10)
$$

where $\bar{c}_j$s and $\bar{c}_e$ are the complex coefficients of quantum levels in the interaction picture, $|\bar{\psi}\rangle = \sum \bar{c}_j |\bar{j}\rangle + \bar{c}_e |\bar{e}\rangle$.

By adiabatically eliminating the excited level, i.e. putting $\dot{\bar{c}}_e = 0$, the system of equations reduces to the lower energy subspace and reads

$$
\dot{\bar{c}}_k = \frac{i\Omega^2}{4\Delta} \sum_{j=1}^3 \bar{c}_j \quad \text{for} \quad k = 1, 2, 3
\qquad (2.11)
$$

This gives rise to the effective Hamiltonian in the ground state subspace:

$$
\bar{H}_{eff} = -\frac{\Omega^2}{4\Delta} \begin{bmatrix}
1 & 1 & 1 \\
1 & 1 & 1 \\
1 & 1 & 1
\end{bmatrix}
\qquad (2.12)
$$

14

$\bar{H}_{eff}$ has Fourier basis as its eigenstates

$$|\bar{\phi}_k\rangle = \frac{1}{\sqrt{3}} \sum_{j=1}^{3} \eta^{kj} |\bar{j}\rangle \quad \text{where} \quad \eta = e^{i\frac{2\pi}{3}} \tag{2.13}$$

The state $|\bar{\phi}_3\rangle$ corresponds to the eigenvalue $\bar{E}_3 = -\frac{3\Omega^2}{4\Delta}$ whereas the other two eigenstates span degenerate subspace with eigenvalue $\bar{E}_{1,2} = 0$. For atoms initially prepared in state $|1\rangle$, the shortest time to evolve to an even superposition of all the three ground states is:

$$\tau = \frac{8\pi\Delta}{9\Omega^2} \tag{2.14}$$

It is therefore this duration that we choose for the implementation of the tritter. The corresponding unitary operator of the tritter, in the Schrödinger picture, reads:

$$U_\tau = \frac{1}{\sqrt{3}} \begin{bmatrix} 1 & \eta e^{-i\delta\tau} & \eta e^{-2i\delta\tau} \\ \eta e^{i\delta\tau} & 1 & \eta e^{-i\delta\tau} \\ \eta e^{2i\delta\tau} & \eta e^{i\delta\tau} & 1 \end{bmatrix} \tag{2.15}$$

Its inverse is useful for the closing tritter, since we can then apply the same calculations above to other ground states as input. We obtain the inverse by flipping the sign of the detuning Δ as implied from Eq. 2.12, illustrated in Fig. 2.2 (b).

2.2.3 Blocker

In the three-slit experiment, one can physically block the slit and in this way remove the photons that were propagating along that path. When spatial separations of the paths are unavailable, one has to find alternative strategies. We wish to discuss a few ways of implementing the latter blockers in the atomic system. The aim is to output an unnormalised state where blocked states are "removed" while coherences between unblocked states are unaffected. This is analogous to spatial slit experiments, where photons are removed by the blockers.

State transfer

Conceptually the simplest method of blocking is to transfer the blocked population into a long-lived state outside the $\{|1\rangle, |2\rangle, |3\rangle, |e\rangle\}$ subspace. This method could be implemented using for example metastable excited ${}^3P_0$ states in alkaline-earth-like atoms. Here, the state lifetime is in the range of seconds, well above the entire duration of any realistic experimental protocol. Such transitions are accessed with narrow frequency lasers.

Dephasing

Since the Sorkin's quantity tests certain forms of interference, it is interesting to explore "blocking" realised by dephasing. In this way the population of atoms in a blocked state does not change, but the coherences to this state are removed. Here we show that this method indeed gives $\mathcal{S}^3 = 0$ in an experimentally robust way, i.e. for arbitrary input state and arbitrary measurement.

Mathematically, blocking the jth state is realised by the dephasing map whose action on a general input density matrix is defined as follows:

$$D_j(\rho) = |j\rangle \langle j| \rho |j\rangle \langle j| + (\mathbb{1} - |j\rangle \langle j|)\rho(\mathbb{1} - |j\rangle \langle j|) \qquad (2.16)$$

where $\mathbb{1}$ denotes identity in the ground-states subspace in Fig. 2.2. The projection operator on jth element removes the off-diagonal elements, while identity keeps the rest of the state intact. When more than one state is blocked, we add more projections onto the required elements. Finally, we note the following identity:

$$\mathcal{D}^3 = \rho - D_1(\rho) - D_2(\rho) - D_3(\rho) + D_{12}(\rho) + D_{13}(\rho) + D_{23}(\rho) - D_{123}(\rho) = \mathbf{0} \qquad (2.17)$$

where $\mathbf{0}$ is the zero matrix. The matrix notation of Eq. 2.17 is:

$$
\mathcal{D}^3 = \begin{bmatrix} \rho_{11} & \rho_{12} & \rho_{13} \\ \rho_{21} & \rho_{22} & \rho_{23} \\ \rho_{31} & \rho_{32} & \rho_{33} \end{bmatrix}
$$

$$
- \begin{bmatrix} \rho_{11} & 0 & 0 \\ 0 & \rho_{22} & \rho_{23} \\ 0 & \rho_{32} & \rho_{33} \end{bmatrix} - \begin{bmatrix} \rho_{11} & 0 & \rho_{13} \\ 0 & \rho_{22} & 0 \\ \rho_{31} & 0 & \rho_{33} \end{bmatrix} - \begin{bmatrix} \rho_{11} & \rho_{12} & 0 \\ \rho_{21} & \rho_{22} & 0 \\ 0 & 0 & \rho_{33} \end{bmatrix}
$$

$$
+ \begin{bmatrix} \rho_{11} & 0 & 0 \\ 0 & \rho_{22} & 0 \\ 0 & 0 & \rho_{33} \end{bmatrix} + \begin{bmatrix} \rho_{11} & 0 & 0 \\ 0 & \rho_{22} & 0 \\ 0 & 0 & \rho_{33} \end{bmatrix} + \begin{bmatrix} \rho_{11} & 0 & 0 \\ 0 & \rho_{22} & 0 \\ 0 & 0 & \rho_{33} \end{bmatrix}
$$

$$
- \begin{bmatrix} \rho_{11} & 0 & 0 \\ 0 & \rho_{22} & 0 \\ 0 & 0 & \rho_{33} \end{bmatrix} = \begin{bmatrix} 0 & 0 & 0 \\ 0 & 0 & 0 \\ 0 & 0 & 0 \end{bmatrix} \qquad (2.18)
$$

which ensures that $\mathcal{S}^3 = 0$ for arbitrary measurement. Note that this equation looks very similar to Eq.1.6. In fact Eq. 1.6 is the trace of Eq. 2.18 multiplied by a projector M that represents a valid measurement.

$$\mathcal{S}^3 = \text{Tr}(M\mathcal{D}^3) = 0 \qquad (2.19)$$

For comparison, let us calculate operator analogous for the "state-transfer method", which will also be called the elimination method:

$$
\begin{aligned}
\mathcal{B}^3 = &\begin{bmatrix} \rho_{11} & \rho_{12} & \rho_{13} \\ \rho_{21} & \rho_{22} & \rho_{23} \\ \rho_{31} & \rho_{32} & \rho_{33} \end{bmatrix} \\
&- \begin{bmatrix} 0 & 0 & 0 \\ 0 & \rho_{22} & \rho_{23} \\ 0 & \rho_{32} & \rho_{33} \end{bmatrix} - \begin{bmatrix} \rho_{11} & 0 & \rho_{13} \\ 0 & 0 & 0 \\ \rho_{31} & 0 & \rho_{33} \end{bmatrix} - \begin{bmatrix} \rho_{11} & \rho_{12} & 0 \\ \rho_{21} & \rho_{22} & 0 \\ 0 & 0 & 0 \end{bmatrix} \\
&+ \begin{bmatrix} 0 & 0 & 0 \\ 0 & 0 & 0 \\ 0 & 0 & \rho_{33} \end{bmatrix} + \begin{bmatrix} 0 & 0 & 0 \\ 0 & \rho_{22} & 0 \\ 0 & 0 & 0 \end{bmatrix} + \begin{bmatrix} \rho_{11} & 0 & 0 \\ 0 & 0 & 0 \\ 0 & 0 & 0 \end{bmatrix} \\
&- \begin{bmatrix} 0 & 0 & 0 \\ 0 & 0 & 0 \\ 0 & 0 & 0 \end{bmatrix} = \begin{bmatrix} 0 & 0 & 0 \\ 0 & 0 & 0 \\ 0 & 0 & 0 \end{bmatrix}
\end{aligned}
\tag{2.20}
$$

We want to focus on the last term. In both cases, it represents the output when all paths are blocked, and is equivalent to absence of input in Eq. 2.20, which allowed us to omit it in Eq. 1.6. However, this is not the case for Eq. 2.18 and we must include it for $\mathcal{S}^3 = 0$. Experimentally, it means that we could do only 7 experiments for elimination-based procedure, and 8 for dephasing-based methods (the same will be true for the spontaneous emission method describe in the next section).

One possibility to realise controlled dephasing is to use lasers with different Rabi frequencies in different realisations of the experiment, or applied for different amount of time, or different detunings. Consider a laser that couples only state $|j\rangle$ to the excited state. By following the steps in Subsec. 2.2.2 one finds that the populations of the ground states are not modified, but state $|j\rangle$ acquires a phase $\Omega_j^2 t/4\Delta$. Therefore, averaging over different realisations of the experiment averages over Ω_j or t or Δ and hence removes coherences to the jth state. Removal of coherences to more than one state could be done sequentially.

Spontaneous emission

Our last blocking procedure exploits spontaneous emission as an incoherent process, removing coherences to a given state. The spontaneous emission process occurs naturally and hence this method is likely the simplest to implement among the three suggestions. We consider blocking by coupling the relevant states to the excited levels with the help of resonant lasers. All the population of the blocked states is then simultaneously transferred to
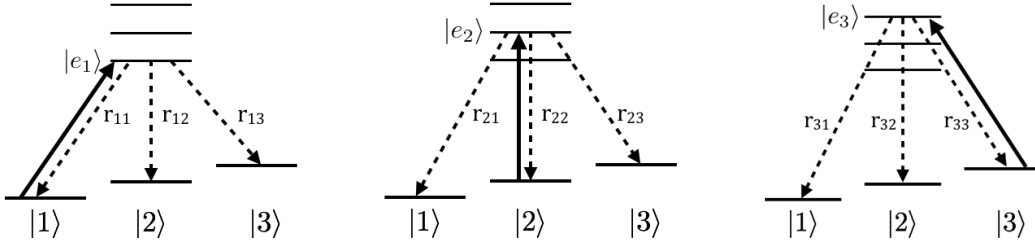
Figure 2.3: "Blocking" of states via spontaneous emission. The resonant laser moves the population of the jth ground state $|j\rangle$ to the jth excited state $|e_j\rangle$. From each excited state, the atoms incoherently decay to all of the ground states with probabilities r_{jk} for transition from jth excited state to the kth ground state.

distinct excited states, from which it spontaneously decays to the ground states. For example, consider blocking state $|2\rangle$ as in the middle of Fig. 2.3. The population of this state is brought to the excited level $|e_2\rangle$ and it then incoherently decays back with rates r_{21}, r_{22} and r_{23} to states $|1\rangle$, $|2\rangle$ and $|3\rangle$ respectively. Therefore, if p_2 was the probability to find the atom initially in state $|2\rangle$, after this process the atom is in this state with probability $r_{22}p_2$. Since spontaneous emission is incoherent, all off-diagonal elements of the density matrix in the second row and column are reduced to zero. The other populations increase in effect of this blocking, e.g. the portion $r_{21}p_1$ is added to p_1. Altogether, the quantum map realising this form of blocking of the jth state is given by

$$E_j(\rho) = (\mathbb{1} - |j\rangle\langle j|)\rho(\mathbb{1} - |j\rangle\langle j|) + \sum_{m=1}^{3} r_{jm}|m\rangle\langle j|\rho|j\rangle\langle m| \qquad (2.21)$$

Similarly, simultaneous blocking of pairs of states j and k is encoded by the map

$$E_{jk}(\rho) = (\mathbb{1} - |j\rangle\langle j| - |k\rangle\langle k|)\rho(\mathbb{1} - |j\rangle\langle j| - |k\rangle\langle k|) \qquad (2.22)$$

$$+ \sum_{m=1}^{3} r_{jm}|m\rangle\left(\langle j|\rho|j\rangle + \sum_{m=1}^{3} r_{km}|m\rangle\langle k|\rho|k\rangle\right. \qquad (2.23)$$

Blocking all the states moves all the atoms to the excited state and hence the resulting density matrix after spontaneous emission is diagonal, with

elements updated as follows:

$$\rho_{mm} = \sum_{j=1}^{3} \rho_{jj} r_{jm} \tag{2.24}$$

$$\rho_{mn} = 0 \quad \text{for} \quad m \neq n \tag{2.25}$$

With this at hand one verifies that analogous identity to the one in Eq. 2.17 holds.

$$\mathcal{E}^3 = \rho - E_1(\rho) - E_2(\rho) - E_3(\rho) + E_{12}(\rho) + E_{13}(\rho) + E_{23}(\rho) - E_{123}(\rho) = \mathbf{0} \tag{2.26}$$

There is a for-curiosity question, whether $\mathcal{S}^3 = 0$, if the excitation-decay cycle is repeated more times, each time waiting long enough between the cycles to ensure that all of the population has indeed been spontaneously decayed. The answer is negative. Repeating this cycle three times produces non-zero Sorkin's quantity, i.e.

$$\rho - E_1^3(\rho) - E_2^3(\rho) - E_3^3(\rho) + E_{12}^3(\rho) + E_{13}^3(\rho) + E_{23}^3(\rho) - E_{123}^3(\rho) \neq \mathbf{0} \tag{2.27}$$

where $E_j^3(\rho) = E_j(E_j(E_j(\rho)))$. Systems with 4 and 5 ground states were calculated as well, and they give non-zero $\mathcal{S}^{4/5}$ after 4 and 5 cycles respectively. This strongly hints at a generalization that starting in a system with N ground states gives non-vanishing $\mathcal{S}^N$ after applying the cycle N times.

2.2.4 Measurement

After the blockers, the remaining atoms are allowed to freely evolve for time T, after which they are measured with the combination of the closing tritter and a detector monitoring the population in state $|1\rangle$. If the state after the free evolution is denoted by ρ the probability that the detector clicks is given by

$$\begin{aligned} p_c &= \langle 1 | U_\tau^{-1} \rho (U_\tau^{-1})^\dagger | 1 \rangle \\ &= \langle 1 | U_\tau^\dagger \rho U_\tau | 1 \rangle \end{aligned} \tag{2.28}$$

The measurement can be achieved with a nuclear spin-sensitive shadow imaging technique [23]. The shadow laser shines on the atom from the individual ground states with low intensity, such that optical pumping can be safely ignored. The schematics is shown below.
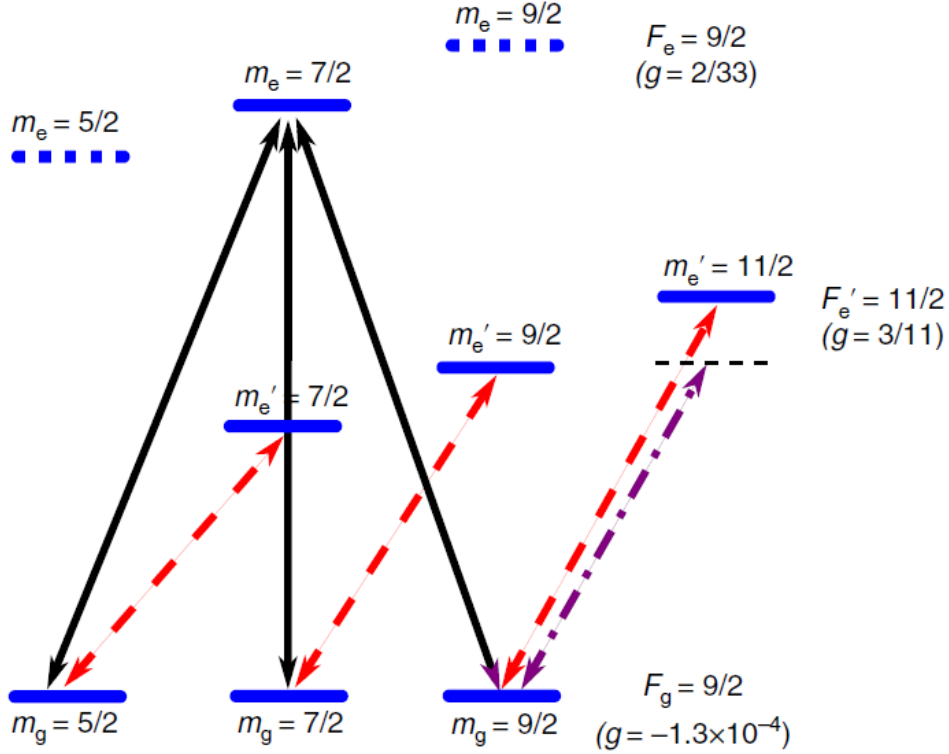
Figure 2.4: Energy levels and experimentally relevant transitions. A magnetic bias field $B = 67G$ lifts the degeneracy of the different Zeeman manifolds and allows to address each transition individually. The Landé factors g are indicated for each hyperfine level. The black arrows correspond to the tripod beams. The dashed red arrows indicate the transitions used for the shadow spin-sensitive imaging system. The dash-dotted purple arrow is the red-detuned cooling transition used in the far off-resonant dipole trap. Image taken from [23].

We have now covered all the elements of the atomic setup presented in Fig. 2.1 and we are in position to present results of its simulations.

2.3 Simulation

We calculate interference fringes expected in the setup for arbitrary δ and T, discuss various sources of noise and estimate the figure of merit κ [8, 11].
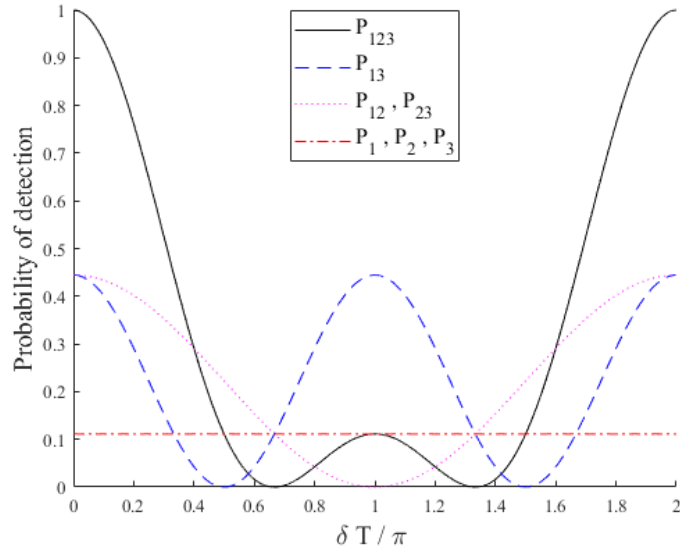
2.3.1   Fringes

Figure 2.5: Interference fringes for various combinations of blocked states. The blockers erase the corresponding part in the superposition of their input state. See Subsec. 2.2.3.

Fig. 2.5 and Fig. 2.6 show predicted interference fringes for various combinations of blocked states. We plot them as a function of the product δT. Therefore, for higher external magnetic field, i.e. higher δ, the full fringe is observed in shorter time. Note that the two blocking methods based on removing coherences only instead of population give rise to exactly the same interference patterns. We also note that the interference pattern obtained by blocking the second state, P_{13}, is twice as fast as the patterns P_{12} and P_{23}. This is expected as the energy difference between pair $\{|1\rangle, |3\rangle\}$ is double the difference between pairs $\{|1\rangle, |2\rangle\}$ or $\{|2\rangle, |3\rangle\}$. We also derived the analytic
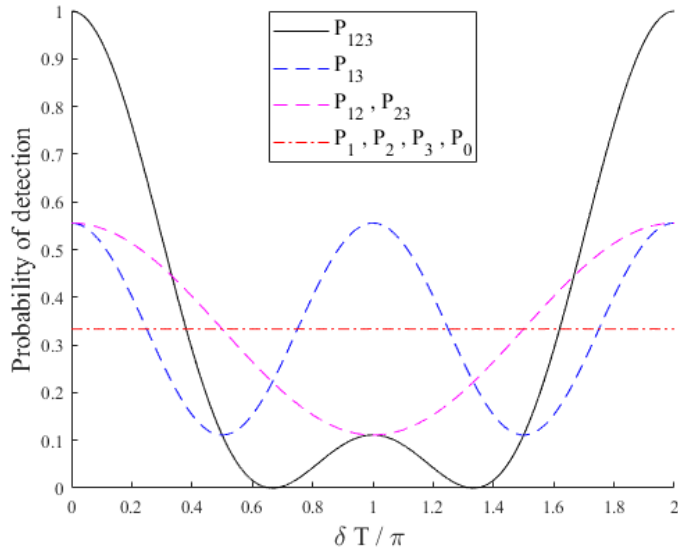
Figure 2.6: Interference fringes for various combinations of blocked states. The blockers are realised by dephasing or spontaneous emission. Both blocking methods lead to the same fringe patterns. See Subsec. 2.2.3.

expressions of the fringes:

$$P_{123} = \frac{1}{9}(3 + 4\cos(\delta\tau) + 2\cos(2\delta\tau)) \tag{2.29a}$$

$$P_{12} = \frac{2}{9}(1 + \cos(\delta\tau)) \tag{2.29b}$$

$$P_{13} = \frac{2}{9}(1 + \cos(2\delta\tau)) \tag{2.29c}$$

$$P_{23} = \frac{2}{9}(1 + \cos(\delta\tau)) \tag{2.29d}$$

$$P_1 = P_2 = P_3 = \frac{1}{9}, \qquad P_0 = 0 \qquad \text{elimination} \tag{2.29e}$$

$$P_1 = P_2 = P_3 = P_0 = \frac{1}{3} \qquad \text{dephasing/spontaneous emission} \tag{2.29f}$$

2.3.2 Noises

Each box in Fig. 2.1 is subject to noise. The Sorkin's quantity is experimentally-friendly in a sense that it vanishes for all initial states and all measurements. Therefore, common systematic effects, present in every experimental run, do not contribute to the estimation of $\mathcal{S}^3$. We shall discuss them individually and identify their contributions to the noise. The dominant factor turns out

to be the finite sample size.

Undefined phases

Consider the first tritter which in different experimental runs prepares states with slightly different relative phases, i.e. instead of the ideal state we obtain the state

$$|\psi\rangle = \frac{1}{\sqrt{3}}(|1\rangle + \eta e^{i\delta\tau}e^{i\phi_2}|2\rangle + \eta e^{i2\delta\tau}e^{i\phi_3}|3\rangle) \tag{2.30}$$

where ϕ_2 and ϕ_3 are the unknown phases. This noise is not important because after averaging over the phases we effectively deal with a mixed state after the tritter. For example, if ϕ_2 and ϕ_3 are normally distributed about zero, the net effect of their randomness is reduction of the off-diagonal elements of $|\psi\rangle\langle\psi|$ by a factor $\exp(\frac{-v}{2})$, where v is the variance of the gaussian. If there are no further errors in the setup, the Sorkin's quantity equals to zero due to Eq. 2.17.

Fluctuation of magnetic field

The fringes in Subsec. 2.3.1 are subjected to fluctuation of magnetic field δ and time T, but the experimental setup has insignficant time uncertainty. We assume the magnetic field is normally distributed about value μ. We start with Eq. 2.29 for the perfect time evolution. Let's assume that $\delta = \varepsilon + \mu \sim N(\mu, \sigma^2)$, where $\varepsilon \sim N(0, \sigma^2)$. Under these assumptions, we calculate the mean and variance of the $\mathcal{S}^3$ due to fluctuation of magnetic field during free evolution between the blockers and the second tritter. We start with some basic statistical formulae.

$$\mathbb{E}[c] = c \quad \text{where c is a constant} \tag{2.31}$$
$$\text{Var}[c] = 0 \tag{2.32}$$

which immediately imply that $\mathbb{E}[P_1, P_2, P_3] = \frac{1}{9}$ or $\frac{1}{3}$, and $\text{Var}[P_1, P_2, P_3, P_0] = 0$. Next we use the moment-generating function of normal distribution and calculate the mean of complex variable $e^{iX} = \cos(X) + i\sin(X)$;

$$\mathbb{E}[e^{itX}] = e^{\mu t - \sigma^2 t^2/2} \tag{2.33}$$

where μ, σ are the mean and standard deviation of variable X respectively. Now consider the real and imaginary part separately

$$\mathbb{E}[\cos(\varepsilon)] = e^{\frac{-\sigma^2}{2}} \tag{2.34}$$
$$\mathbb{E}[\sin(\varepsilon)] = 0 \tag{2.35}$$

Next, the following basic trigonometric formulae are used to obtain expectation value of $\cos(\delta T)$

$$\cos(\delta T) = \cos((\varepsilon + \mu)T) = \cos(\varepsilon T)\cos(\mu T) - \sin(\varepsilon T)\sin(\mu T)$$

$$\mathbb{E}[\cos(\delta T)] = \cos(\mu T)e^{-\frac{(\sigma T)^2}{2}} \tag{2.36}$$

which means that the fluctuation of magnetic field will result in expectation value difference of $1 - e^{-\frac{(\sigma T)^2}{2}} \approx \frac{(\sigma T)^2}{2}$. But at the same time, all of the summands in Eq. 2.29 are multiplied by the same factor and then subtracted, the net effect on $\mathbb{E}[\mathcal{S}^3]$ is cancelled out.

For the variance, we obtain:

$$\cos^2(\delta T) = \frac{1 + \cos(2\delta T)}{2}$$

$$\mathrm{Var}[\cos(\delta T)] = \mathbb{E}[\cos^2(\delta T)] - (\mathbb{E}[\cos(\delta T)])^2$$

$$= \frac{1}{2}(1 + e^{-\frac{(2\sigma T)^2}{2}}\cos(2\mu T) - 2e^{-\frac{(\sigma T)^2}{2}\cdot 2}\cos^2(\mu T))$$

$$= \frac{1}{2}(1 + e^{-2(\sigma T)^2}\cos(2\mu T) - 2e^{-(\sigma T)^2}\cos^2(\mu T)) \tag{2.37}$$

$$\mathrm{Var}[\mathcal{S}^3] = \mathrm{Var}[P_{123}] + \mathrm{Var}[P_{12}] + \mathrm{Var}[P_{13}] + \mathrm{Var}[P_{23}]$$

$$= \mathrm{Var}[\frac{4 \cdot 2}{9}\cos(\delta T)] + \mathrm{Var}[\frac{2 \cdot 2}{9}\cos(2\delta T)]$$

$$= \mathrm{Var}[\frac{8}{9}\cos(\delta T)] + \mathrm{Var}[\frac{4}{9}\cos(2\delta T)] \tag{2.38}$$

If we demand the variance of $\mathcal{S}^3$ to be of the order 10^{-7}, σ only needs to be smaller than 10^{-2} under the worst case scenario assumptions.

Spontaneous emission: phase change

For the blocking method with spontaneous emission, we assumed that by blocking a single path, the coherence of the other two paths are unaffected. For example, if we block the first path:

$$\rho = \begin{bmatrix} \rho_{11} & \rho_{12} & \rho_{13} \\ \rho_{21} & \rho_{22} & \rho_{23} \\ \rho_{31} & \rho_{32} & \rho_{33} \end{bmatrix} \tag{2.39}$$

$$B_1(\rho) = \begin{bmatrix} 0 & 0 & 0 \\ 0 & \rho_{22} & \rho_{23} \\ 0 & \rho_{32} & \rho_{33} \end{bmatrix} \tag{2.40}$$

However, due to AC-Stark shift, we expect the phase of the coherence term to change, i.e.

$$B_1(\rho) = \begin{bmatrix} 0 & 0 & 0 \\ 0 & \rho_{22} & \rho_{23}e^{-i\phi_1} \\ 0 & \rho_{32}e^{i\phi_1} & \rho_{33} \end{bmatrix} \qquad (2.41)$$

this phase change is only present on the three single-path blockers, since double-path blockers remove all coherence terms. This combined with the fact that all single-path-blocker probabilities enter with negative terms in Eq. 2.26, means that any non-zero phase $\phi_{1,2,3}$ will make $\mathcal{S}^3 \neq 0$. We can rewrite Eq. 2.29 to include the changes and estimate the error on $\mathcal{S}^3$ without further simulations:

$$P_{123} = \frac{1}{9}(3 + 4\cos(\delta T) + 2\cos(2\delta T)) \qquad (2.42a)$$

$$P_{23} = \frac{2}{9}(1 + \cos(\delta T - \phi_1)) \qquad (2.42b)$$

$$P_{13} = \frac{2}{9}(1 + \cos(2\delta T - \phi_2)) \qquad (2.42c)$$

$$P_{12} = \frac{2}{9}(1 + \cos(\delta T - \phi_3)) \qquad (2.42d)$$

$$P_1 = P_2 = P_3 = \frac{1}{9} \qquad (2.42e)$$

$$\begin{aligned} \mathcal{S}^3 = \frac{2}{9}(&2\cos(\delta T) + \cos(2\delta T) \\ &- \cos(\delta T - \phi_1) \\ &- \cos(2\delta T - \phi_2) \\ &- \cos(\delta T - \phi_3)) \end{aligned} \qquad (2.42f)$$

For small $\phi_{1,2,3}$, we can estimate the error on $\mathcal{S}^3$ is on the same order as $|\phi_j|$.

Finite sample size

Any experiment can only be repeated a finite number of times and this influences precision of estimated parameters. In our proposed setup the final measurement establishes whether the atom is in the initial state or not. The outcome is accordingly binary and after N repetitions of the experiment, the estimated probability that detector clicks is proportional to $N \cdot p \pm \sqrt{N \cdot p(1-p)}$, where $N \cdot p$ is the mean of the binomial distribution with p being the quantum mechanical probability of the click and the error of $\sqrt{N \cdot p(1-p)}$ is characterised by the standard deviation of this binomial

distribution. Since quantum mechanics predicts $\mathcal{S}^3 = 0$, on average this value will appear after N experimental runs, but with the error bar scaling as $\sqrt{N}$. At the same time, the double-slit interferences $\mathcal{S}_{jk}^2$, see Eq. 2.1, have leading terms proportional to N as quantum mechanical double-slit interference does not vanish. Therefore, finite sample size of N measurement outcomes gives rise to the value of the figure of merit κ with error bar on the order $\frac{1}{\sqrt{N}}$. A typical cloud in cold atom experiments contains about 10^5 independent atoms and the average over this many individual quantum systems is realised in a single experimental run. Such a singe run, from producing the cloud to the final measurement outcome, takes less than 1 second. Within two weeks one can therefore conduct 6×10^5 such experiments bringing the total sample size to 10^{10} and the precision of κ down to the order 10^{-5}.

2.4 Summary

We have discussed various ways to implement analogues of triple-slit experiments with atoms. Such experiments could test the Born rule in previously unexplored domain and could bound non-quantum parameters in generalisations of quantum mechanics including higher-order interference, e.g. in the density cube model introduced later. Due to parallel processing of many atoms in a single experimental run, the scheme considered offers an order of magnitude improvement in the precision of testing higher-order interference over the previous results.

Chapter 3

Interference of indistinguishable particles

Quantum mechanics is usually described as "linear", in two-fold sense. The states $|s\rangle$ can always be decomposed into linear superpositions of basis vectors $|j\rangle$, and operators Os on the said states are also linear:

$$|s\rangle = \sum_j c_j |j\rangle \tag{3.1a}$$

$$O(|s_1\rangle + |s_2\rangle) = O(|s_1\rangle) + O(|s_2\rangle) \tag{3.1b}$$

which together gives us the desired property

$$O(|s\rangle) = \sum_j c_j O |j\rangle \tag{3.2}$$

We show in this chapter that there is no third- and higher-order interferences in quantum mechanics of individual particles. However, in second quantization, higher-order interference emerged in canonical quantum mechanics and witnesses non-linear transformations of mode operators. Other forms of non-linearity, e.g. non-linear Schrödinger equations [27–29] or non-linear detectors [30] also lead to non-zero higher-order Sorkin's quantity.

3.1 All linear processes lead to vanishing higher-order interference

First we show that all linear processes give rise to only second order interference, i.e. $\mathcal{S}^3 = 0$ independent of the input multipartite state. We consider a beam of indistinguishable particles in an arbitrary input state ρ with M
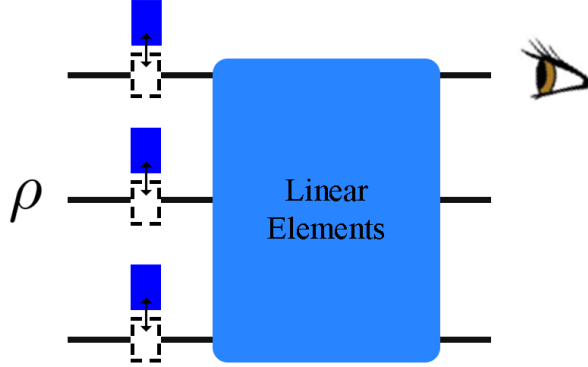
Figure 3.1: Example of linear optical experiment with $M = 3$. The paths can be individually blocked. The black box represents any linear processes, e.g. beam-splitters, mirrors etcetera, and their combinations. The output from the first path is measured at the end.

paths in the setup. The particle number does not have to be well defined, e.g. the input could be a coherent state of photons. With each path we associate local Fock space $\mathcal{H}_M$ spanned by Fock states $|n\rangle_m$ describing n excitations (photons) in the m-th path (mode). The entire Hilbert space of this system is therefore a tensor product $\mathcal{H}_1 \otimes \mathcal{H}_2 \otimes \cdots \otimes \mathcal{H}_m$ and we need to specify how blocking of paths is encoded in this formalism. Blocking the m-th path has the effect:

$$B_m = (\mathbb{1} - |n\rangle_m \langle n|)\rho(\mathbb{1} - |n\rangle_m \langle n|) \tag{3.3}$$

i.e. it produces vacuum in the blocked path and removes coherence from all the other paths, without re-normalizing the state. If we place the final detector along the first path, see Fig. 3.1, the intensities can be computed as:

$$I = \mathrm{Tr}(a_1^\dagger a_1 U B(\rho) U^\dagger) \tag{3.4}$$

where $a_1^\dagger a_1$ is the number operator in $\mathcal{H}_1$ and B is the blocking map. Since the same measurement is conducted for all the combinations of blocked paths, we introduce an "interference operator" to sum all combinations of blocking.

$$\hat{I}_M = B_0(\rho) - B_1(\rho) - B_2(\rho) + \cdots (-1)^M B_{123\cdots M}(\rho) \tag{3.5}$$
$$I_M = \mathrm{Tr}(U^\dagger a_1^\dagger a_1 U \hat{I}_M) \tag{3.6}$$

where the sign for each term follows Eq. 1.7. The Sorkin's quantity can then be calculated from Eq. 3.6. Any linear process satisfies

$$U^\dagger a_j U = \sum_m u_{jm} a_m \tag{3.7}$$

for all j, where u_{jm} are the complex coefficients and accordingly:

$$\mathcal{S}^M = \text{Tr}(\sum_{m,m'} u_{jm} a_m^\dagger a_{m'} u_{m'j'}^* \hat{I}_M) = 0 \tag{3.8}$$

where in the last equation we used the fact that the interference operator vanishes under partial trace over any path, i.e. $\text{Tr}_k(\hat{I}_M) = 0$ where the partial trace is over arbitrary non-empty set k. Note that non-linearity is necessary for higher-order interference, but not sufficient. For example, a non-linear process mapping $a^\dagger$ to a sum of squared operators $\sum_m a_m^\dagger a_m^\dagger$ still admits $\mathcal{S}^M = 0$, because in Eq. 3.8 each term in the sums couples only two paths and hence the partial trace argument gives vanishing $\mathcal{S}^M$. Accordingly, experimental verification of non-zero $\mathcal{S}^M$ indicates multi-mode coupling in the underlying process (could be completely unknown) and provides the minimal number of the coupled paths.

3.2 Non-linear quantum optics and higher-order interference

Optical Kerr effect is a phenomenon in transparent materials in which the refractive index changes in response to an applied electric field. Such changes are usually small, on the order of $10^{-16}\,cm\,W$ for silica glass, and so they are difficult to observe. However, there are materials and techniques for which the effect is much higher, at $10^{-5}\,cm\,W$ [31, 32], allowing experiments with much weaker laser strength.

Possible design of three-path optical experiment producing non-zero $\mathcal{S}^3$ is described below in Fig. 3.2. This is by no means the only way of doing so. However we chose it over other designs for ease of calculation and large Sorkin's quantity. Refer to Appendix. A.1 for comparison. The non-linear element NL, whose action is described by a non-linear phase shift operator U_{jk}, is defined as:

$$U_{jk}^\dagger a_j U_{jk} = e^{i\theta a_k^\dagger a_k} a_j \tag{3.9a}$$

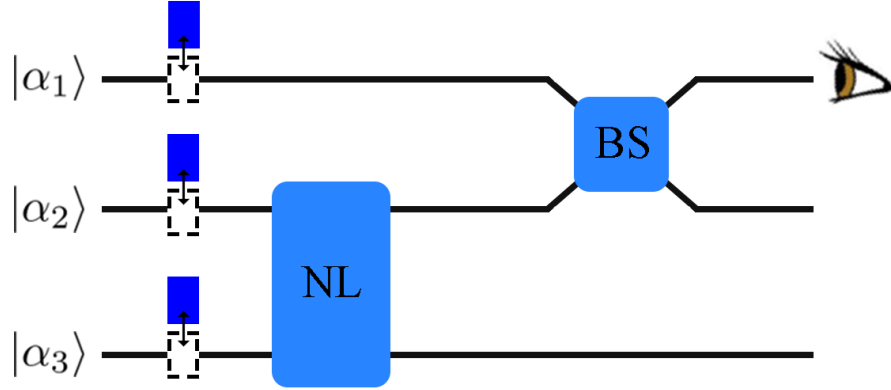$$U_{jk}^\dagger a_j^\dagger U_{jk} = e^{-i\theta a_k^\dagger a_k} a_j \tag{3.9b}$$

Figure 3.2: Experimental design of three-path optical experiment producing $\mathcal{S}^3 \neq 0$. The inputs are three lasers described by coherent states $|\alpha_j\rangle$. Blocker for each path can be independently inserted. NL is the non-linear media described by Eq. 3.9. BS is a standard 50-50 beam-splitter. The output from the first path is measured at the end.

where θ is the strength of non-linearity.

The beam-splitter BS whose action is described by operator S_{jk} acts as:

$$S_{jk}^\dagger a_j^\dagger S_{jk} = \frac{1}{\sqrt{2}}(a_j^\dagger + a_k^\dagger) \tag{3.10a}$$

$$S_{jk}^\dagger a_j S_{jk} = \frac{1}{\sqrt{2}}(a_j + a_k) \tag{3.10b}$$

The intensities measured in this setup are:

$$I_{123} = \text{Tr}(U_{23}^\dagger S_{12}^\dagger a_1^\dagger a_1 S_{12} U_{23}\rho)$$

$$= \frac{1}{2}\text{Tr}(U_{23}^\dagger(a_1^\dagger a_1 + a_1^\dagger a_2 + a_2^\dagger a_1 + a_2^\dagger a_2)U_{23}\rho)$$

$$= \frac{1}{2}\text{Tr}((a_1^\dagger a_1 + a_2^\dagger a_2 + a_1^\dagger a_2 e^{i\theta N_3} + a_2^\dagger e^{-i\theta N_3} a_1)\rho)$$

$$= \frac{1}{2}(|\alpha_1|^2 + |\alpha_2|^2 + \langle\alpha_1| a_1^\dagger |\alpha_1\rangle \langle\alpha_2| a_2 |\alpha_2\rangle \langle\alpha_3| e^{i\theta N_3} |\alpha_3\rangle$$

$$+ \langle\alpha_1| a_1 |\alpha_1\rangle \langle\alpha_2| a_2^\dagger |\alpha_2\rangle \langle\alpha_3| e^{-i\theta N_3} |\alpha_3\rangle)$$

$$= \frac{1}{2}(|\alpha_1|^2 + |\alpha_2|^2 + \alpha_1^*\alpha_2 \langle\alpha_3|e^{i\theta}\alpha_3\rangle + \alpha_1\alpha_2^* \langle\alpha_3|e^{-i\theta}\alpha_3\rangle) \qquad (3.11a)$$

$$I_{12} = \text{Tr}(U_{23}^\dagger S_{12}^\dagger a_1^\dagger a_1 S_{12} U_{23} B_3(\rho))$$

$$= \frac{1}{2}\text{Tr}((a_1^\dagger a_1 + a_2^\dagger a_2 + a_1^\dagger a_2 + a_2 a_1)B_3(\rho))$$

$$= \frac{1}{2}(|\alpha_1|^2 + |\alpha_2|^2 + \langle\alpha_1| a_1^\dagger |\alpha_1\rangle \langle\alpha_2| a_2 |\alpha_2\rangle + \langle\alpha_1| a_1 |\alpha_1\rangle \langle\alpha_2| a_2^\dagger |\alpha_2\rangle$$

$$= \frac{1}{2}(|\alpha_1|^2 + |\alpha_2|^2 + \alpha_1^*\alpha_2 + \alpha_1\alpha_2^*) \qquad (3.11b)$$

$$I_{13} = \text{Tr}(U_{23}^\dagger S_{12}^\dagger a_1^\dagger a_1 S_{12} U_{23} B_2(\rho))$$

$$= \frac{1}{2}\text{Tr}((a_1^\dagger a_1 + a_2^\dagger a_2 + a_1^\dagger a_2 + a_2 a_1)B_2(\rho))$$

$$= \frac{1}{2}|\alpha_1|^2 \qquad (3.11c)$$

$$I_{23} = \text{Tr}(U_{23}^\dagger S_{12}^\dagger a_1^\dagger a_1 S_{12} U_{23} B_1(\rho))$$

$$= \frac{1}{2}\text{Tr}((a_1^\dagger a_1 + a_2^\dagger a_2 + a_1^\dagger a_2 e^{i\theta N_3} + a_2^\dagger e^{-i\theta N_3} a_1)B_1(\rho))$$

$$= \frac{1}{2}|\alpha_2|^2 \qquad (3.11d)$$

$$I_1 = I_{13} = \frac{1}{2}|\alpha_1|^2 \qquad (3.11e)$$

$$I_2 = I_{23} = \frac{1}{2}|\alpha_2|^2 \qquad (3.11f)$$

$$I_3 = I_0 = 0 \qquad (3.11g)$$

The corresponding Sorkin's quantity $\mathcal{S}^3$ is calculated as:

$$\mathcal{S}^3 = I_{123} - I_{12} - I_{13} - I_{23} + I_1 + I_2 + I_3 - I_0$$

$$= \frac{1}{2}[\alpha_1^*\alpha_2(\langle\alpha_3|e^{i\theta}\alpha_3\rangle - 1) + \alpha_1\alpha_2^*(\langle\alpha_3|e^{-i\theta}\alpha_3\rangle - 1)] \qquad (3.12)$$

From these calculations, we can observe that experiments have to incorporate non-linearity into all three paths (Eq. 3.11a), either directly by non-linear operators or beam-splitter after non-linear operation, in order to have non-zero Sorkin's quantity. This is not a coincidence and is a direct consequence of Eq. 3.8. If we use "interference operator" in Eq. 3.6, the calculation becomes much simpler.

$$\hat{I}^3 = (|\alpha_1\rangle\langle\alpha_1| - |0_1\rangle\langle0_1|) \otimes (|\alpha_2\rangle\langle\alpha_2| - |0_2\rangle\langle0_2|) \otimes (|\alpha_3\rangle\langle\alpha_3| - |0_3\rangle\langle0_3|)$$

(3.13)

$$\begin{aligned}
\mathcal{S}^3 &= \text{Tr}(U_{23}^\dagger S_{12}^\dagger a_1^\dagger a_1 S_{12} U_{23} \hat{I}^3) \\
&= \frac{1}{2}\text{Tr}(U_{23}^\dagger(a_1^\dagger a_1 + a_1^\dagger a_2 + a_2^\dagger a_1 + a_2^\dagger a_2)U_{23}\hat{I}^3) \\
&= \frac{1}{2}\text{Tr}[(a_1^\dagger a_1 + a_2^\dagger a_2 + e^{-i\theta N_3}a_1^\dagger a_2 + a_2^\dagger a_1 e^{i\theta N_3})\hat{I}^3] \\
&= \frac{1}{2}\langle\alpha_1|a_1^\dagger|\alpha_1\rangle\langle\alpha_2|a_2|\alpha_2\rangle(\langle\alpha_3|e^{-i\theta N_3}|\alpha_3\rangle - \langle0_3|e^{-i\theta N_3}|0_3\rangle) + h.c. \\
&= \frac{1}{2}[\alpha_1^*\alpha_2(\langle\alpha_3|e^{i\theta}\alpha_3\rangle - 1) + \alpha_1\alpha_2^*(\langle\alpha_3|e^{-i\theta}\alpha_3\rangle - 1)]
\end{aligned}$$

(3.14)

which agrees with Eq. 3.12. In addition, it is possible to have zero Sorkin's quantity even with non-linear operation due to symmetry in the setup. For example, the setup below has symmetrical non-linear elements and the non-linearity cancels out exactly. This illustrates that negation of result in Sec. 3.1 is not true, i.e. presence of non-linear elements does not guarantee $\mathcal{S}^3 \neq 0$.
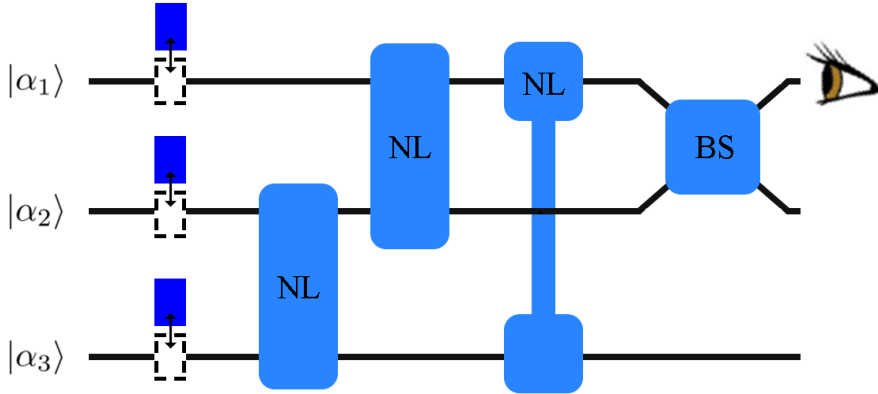

Figure 3.3: Experimental design with three non-linear elements U_{23}, U_{12} and U_{13} of the same strength θ. This configuration produces $\mathcal{S}^3 = 0$.

Note that the order of the non-linear elements is inconsequential due to

32

commutativity between them.

$$[U_{jk}, U_{kl}] = e^{i\theta N_j N_k}e^{i\theta N_k N_l} - e^{i\theta N_k N_l}e^{i\theta N_j N_k}$$
$$= e^{i\theta N_j (N_k)^2 N_l} - e^{i\theta N_l (N_k)^2 N_j} = 0 \tag{3.15}$$

$$I_{123} = \mathrm{Tr}(U_{13}^\dagger U_{12}^\dagger U_{23}^\dagger S_{12}^\dagger a_1^\dagger a_1 S_{12} U_{23} U_{12} U_{13}\rho)$$
$$= \frac{1}{2}\mathrm{Tr}((a_1^\dagger a_1 + a_2^\dagger a_2 + a_1^\dagger e^{-i\theta N_2}e^{-i\theta N_3}a_2 e^{i\theta N_3}e^{i\theta N_1} + a_1 e^{i\theta N_2}e^{i\theta N_3}a_2^\dagger e^{-i\theta N_3}e^{-i\theta N_1}\rho)$$
$$= \frac{1}{2}(|\alpha_1|^2 + |\alpha_2|^2 + \langle \alpha_1| a_1^\dagger e^{i\theta N_1}|\alpha_1\rangle \langle \alpha_2| a_2 e^{-i\theta N_2}|\alpha_2\rangle \langle \alpha_3|\alpha_3\rangle$$
$$+ \langle \alpha_1| a_1 e^{-i\theta N_1}|\alpha_1\rangle \langle \alpha_2| a_2^\dagger e^{i\theta N_2}|\alpha_2\rangle \langle \alpha_3|\alpha_3\rangle)$$
$$= \frac{1}{2}(|\alpha_1|^2 + |\alpha_2|^2 + \alpha_1^* e^{i\theta N_1}\alpha_2 e^{-i\theta N_2} + \alpha_1 e^{-i\theta N_1}\alpha_2^* e^{i\theta N_2}) \tag{3.16a}$$
$$I_{12} = \mathrm{Tr}(U_{13}^\dagger U_{12}^\dagger U_{23}^\dagger S_{12}^\dagger a_1^\dagger a_1 S_{12} U_{23} U_{12} U_{13} B_3(\rho))$$
$$= \frac{1}{2}(|\alpha_1|^2 + |\alpha_2|^2 + \langle \alpha_1| a_1^\dagger e^{i\theta N_1}|\alpha_1\rangle \langle \alpha_2| a_2 e^{-i\theta N_2}|\alpha_2\rangle \langle 0|0\rangle$$
$$+ \langle \alpha_1| a_1 e^{-i\theta N_1}|\alpha_1\rangle \langle \alpha_2| a_2^\dagger e^{i\theta N_2}|\alpha_2\rangle \langle 0|0\rangle)$$
$$= \frac{1}{2}(|\alpha_1|^2 + |\alpha_2|^2 + \alpha_1^* e^{i\theta N_1}\alpha_2 e^{-i\theta N_2} + \alpha_1 e^{-i\theta N_1}\alpha_2^* e^{i\theta N_2}) \tag{3.16b}$$
$$I_{13} = \mathrm{Tr}(U_{13}^\dagger U_{12}^\dagger U_{23}^\dagger S_{12}^\dagger a_1^\dagger a_1 S_{12} U_{23} U_{12} U_{13} B_2(\rho))$$
$$= \frac{1}{2}|\alpha_1|^2 \tag{3.16c}$$
$$I_{23} = \mathrm{Tr}(U_{13}^\dagger U_{12}^\dagger U_{23}^\dagger S_{12}^\dagger a_1^\dagger a_1 S_{12} U_{23} U_{12} U_{13} B_1(\rho))$$
$$= \frac{1}{2}|\alpha_2|^2 \tag{3.16d}$$
$$I_1 = I_{13} = \frac{1}{2}|\alpha_1|^2 \tag{3.16e}$$
$$I_2 = I_{23} = \frac{1}{2}|\alpha_2|^2 \tag{3.16f}$$
$$I_3 = I_0 = 0 \tag{3.16g}$$

It is easy to verify that $\mathcal{S}^3 = 0$ by the equations above.

Extension into higher-order Sorkin's quantity

We now extend the three-path experimental setup to arbitrary number of paths in order to detect higher-order Sorkin's quantity $\mathcal{S}^n$.
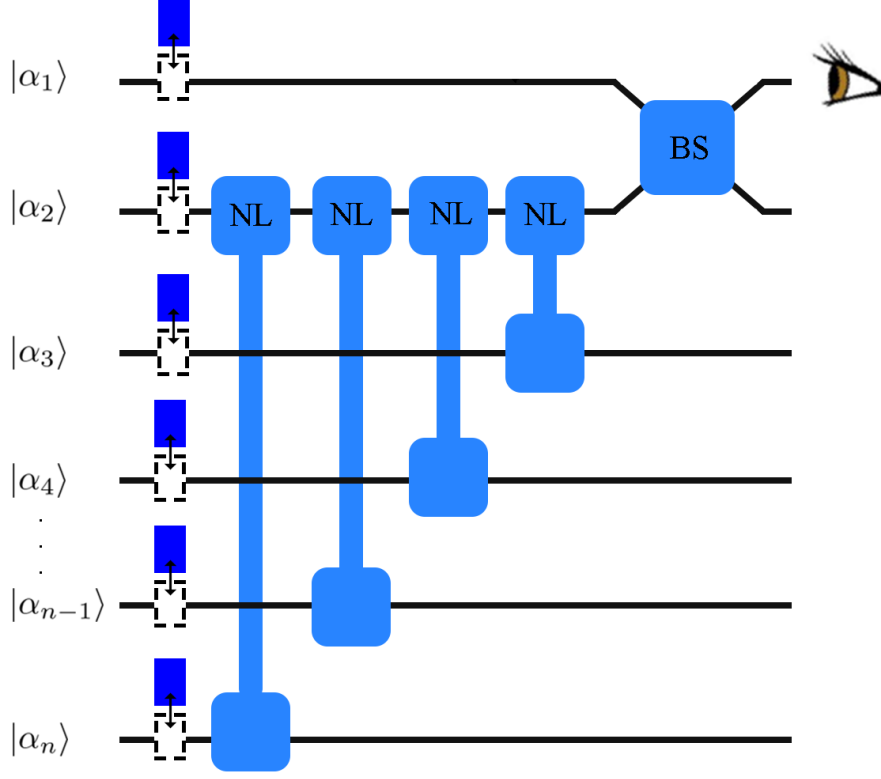We start with four paths first and then generalize to n paths. The forth-order

Figure 3.4: Setup with n paths. The non-linear elements connect path two to all other paths except for the first, where a beam-splitter is placed instead.

interference operator for coherent states as input is:

$$
\begin{aligned}
\hat{I}^4 =& (|\alpha_1\rangle \langle\alpha_1| - |0_1\rangle \langle 0_1|) \otimes (|\alpha_2\rangle \langle\alpha_2| - |0_2\rangle \langle 0_2|) \\
& \otimes (|\alpha_3\rangle \langle\alpha_3| - |0_3\rangle \langle 0_3|) \otimes (|\alpha_4\rangle \langle\alpha_4| - |0_4\rangle \langle 0_4|)
\end{aligned}
\tag{3.17}
$$

The corresponding Sorkin's quantity is:

$$
\begin{aligned}
\mathcal{S}^4 =& \mathrm{Tr}(U_{24}^\dagger U_{23}^\dagger S_{12}^\dagger a_1^\dagger a_1 S_{12} U_{23} U_{24} \hat{I}^4) \\
=& \frac{1}{2}\mathrm{Tr}(U_{24}^\dagger U_{23}^\dagger (a_1^\dagger a_1 + a_1^\dagger a_2 + a_2^\dagger a_1 + a_2^\dagger a_2) U_{23} U_{24} \hat{I}^4) \\
=& \frac{1}{2}\mathrm{Tr}(a_1^\dagger a_1 + a_2^\dagger a_2 + a_1^\dagger a_2 e^{i\theta N_3} e^{i\theta N_4} + a_2^\dagger e^{-i\theta N_3} e^{-i\theta N_4} \, a_1 \hat{I}^4) \\
=& \frac{1}{2}\alpha_1^* \alpha_2 (\langle\alpha_3| e^{i\theta N_3} |\alpha_3\rangle - 1)(\langle\alpha_4| e^{i\theta N_4} |\alpha_4\rangle - 1) + h.c.
\end{aligned}
\tag{3.18}
$$

When compared to $\mathcal{S}^3$ in Eq. 3.12, $\mathcal{S}^4$ simply multiplies one more term. In the same spirit, we can calculate $\mathcal{S}^N$ for the setup in Fig. 3.4 with arbitrary

34

number of paths under the assumption that the laser strength is the same for all paths, i.e. $|\alpha_1|^2 = |\alpha_2|^2 = |\alpha_3|^2 \cdots$.

$$\mathcal{S}^n = \frac{1}{2}\alpha_1^*\alpha_2(\langle\alpha_3|e^{i\theta}\alpha_3\rangle - 1)(\langle\alpha_4|e^{i\theta}\alpha_4\rangle - 1)\cdots + h.c. \tag{3.19}$$

$$= \frac{1}{2}|\alpha|^2(e^{-|\alpha|^2(1-e^{i\theta})} - 1)^{n-2} + h.c. \tag{3.20}$$

where we have used the formula $\langle\alpha|e^{\pm i\theta}\alpha\rangle = e^{-|\alpha|^2(1-e^{\pm i\theta})}$.

3.3   Linear optics with non-linear detectors

Real life photon detectors are imperfect. This effect becomes noticeable in the extremely high intensity regime [30, 33]. We picture a scenario where all experimental apparatus are linear and free from noises, and only the detector has non-linear response. To simulate the effect of such detectors, we make a few natural assumptions based on the response of real detectors [33].

1. The detectors have a sub-linear response to laser intensity.

2. The response is almost linear in low laser intensity range.

3. The overall response curve is at most second order.

3.3.1   Simulating ideal detector

We begin our simulation with coherent superposition of three Gaussian wave packets in free space, evolve them according to standard Schrödinger equation for 1 ms, and repeat the simulation with wave packets removed according to Eq. 1.6 to measure the Sorkin's quantity. The underlying equations for simulation is Runge-Kutta method (RK45) with error tolerance set as 10^{-10}. The results are presented in Fig. 3.5 below. The Sorkin's quantity $\mathcal{S}^3$ is simply the sum of these intensities, with signs alternating whenever the number of slits opened changes, according to Eq. 1.6. It is found to be well below the numerical precision $((10^{-14} \ll 10^{-10})$, see Fig. 3.6), as expected for linear process.
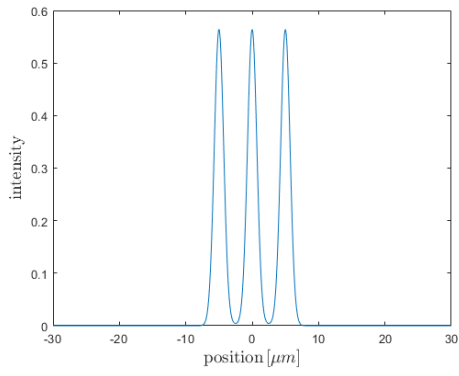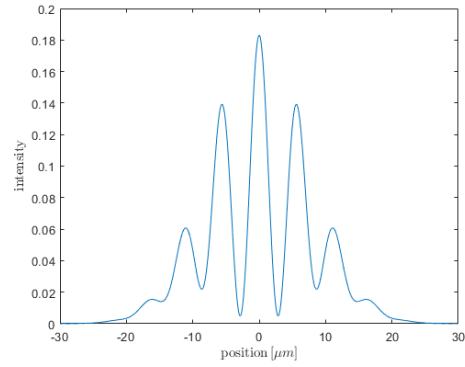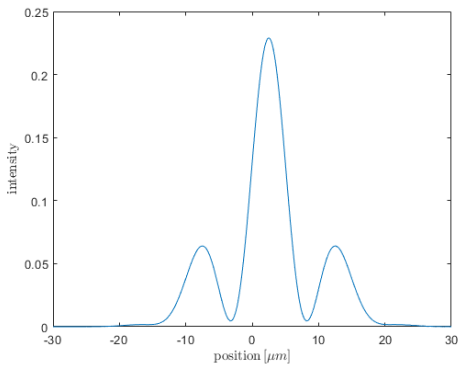
(a) Inital condition
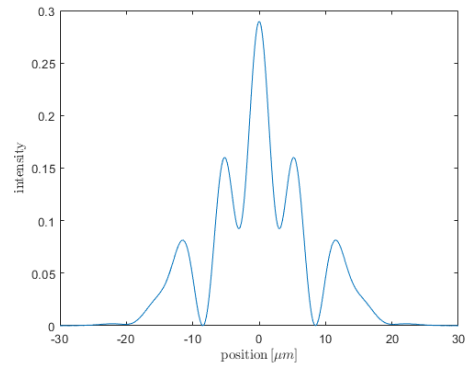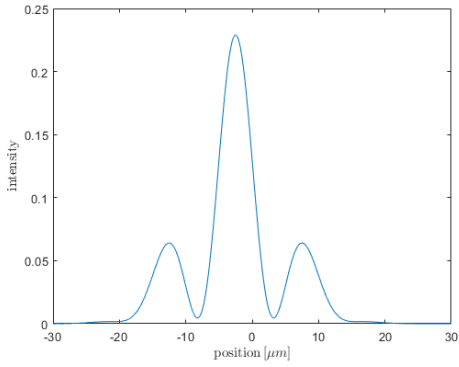
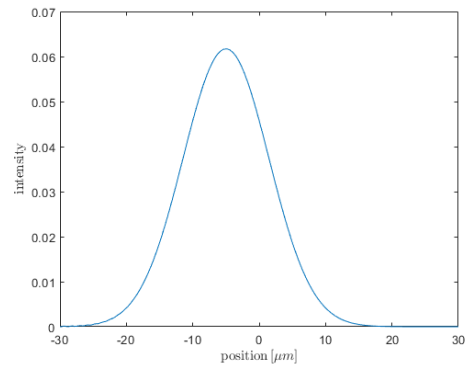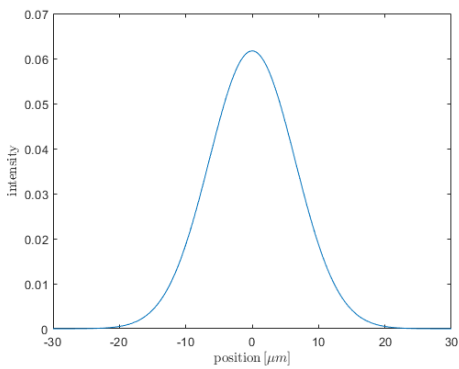(b) All slits open I_{123}

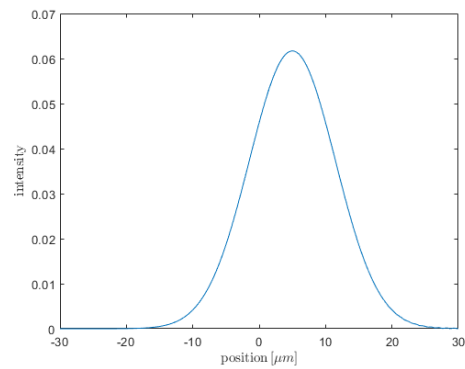(c) Slits 1,2 open I_{12}

(d) Slits 1,3 open I_{13}

(e) Slits 2,3 open I_{23}

(f) Slit 1 open I_1

(g) Slit 2 open I_2

(h) Slit 3 open I_3

Figure 3.5: Intensities for a free quantum particle evolved with standard Schrödinger equation.
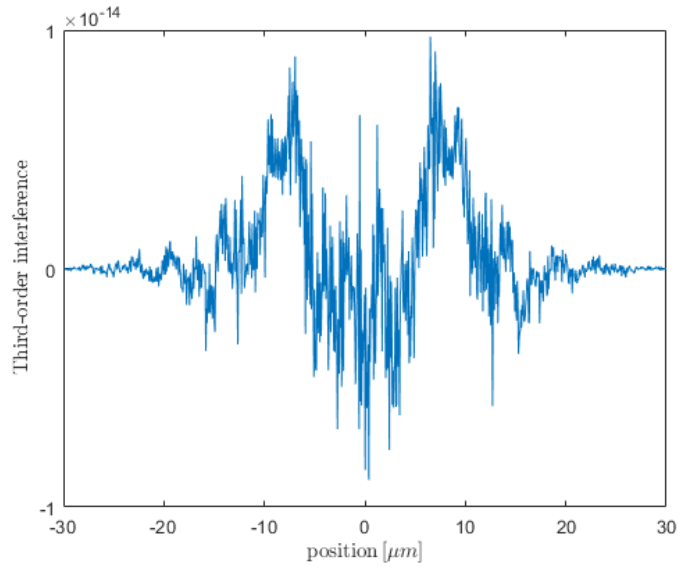
Figure 3.6: Sorkin's quantity for free quantum particle evolved with standard Schrödinger equation. The values are in the order of 10^{-14} which is much smaller than the error tolerance of 10^{-10} that we have set in numerics. That is, the third-order interference is numerical 0.

3.3.2   Simulating non-ideal detector

We use the result above and transform the individual intensities to simulate how a non-ideal detector behaves. The steps are as follows:

1. Using the assumptions, we rescale the intensity as

$$I_{nonlinear} = I_{ideal} - \varepsilon I_{ideal}^2$$

where ε is a small number, and I_{ideal} is intensity at each point of the screen. Effectively, the whole intensity plot decreases in amplitude, but the amount differs, where the "taller" part shrinks more.

2. Compute $\mathcal{S}^3$ by combining the plots again.

3. Repeat with different ε.
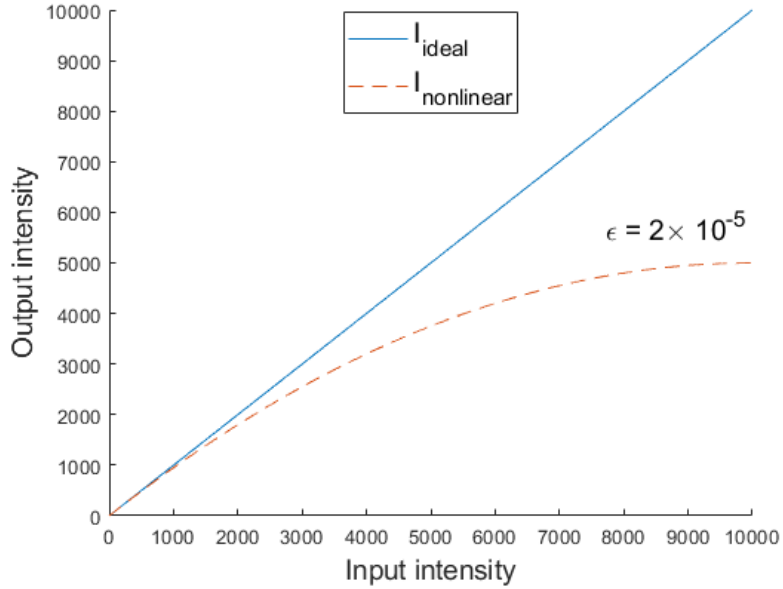
(a) Simulation of ideal vs non-ideal detector for $\varepsilon = 2 \times 10^{-5}$
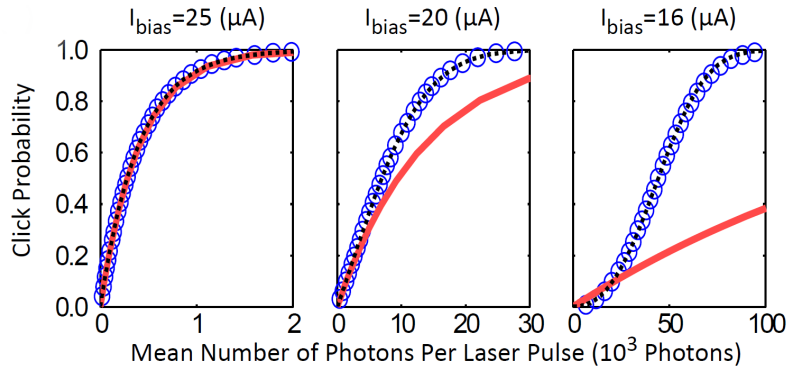
(b) Click probability for a single photon detector at different bias currents. The blue circles are measured click probabilities. Figure taken from [30].

Figure 3.7: The trend from the experimental results matches sufficiently well with our assumption.

We see in the log-log plot in Fig. 3.8 that the magnitude of $\mathcal{S}^3$ follows a nice straight line, with the relation:

$$O(\mathcal{S}^3) \approx O(\varepsilon) - 2 \tag{3.21}$$

Note that the actual number depends heavily on the initial conditions of system, e.g. mass of the particles, but the linear relation is general, under
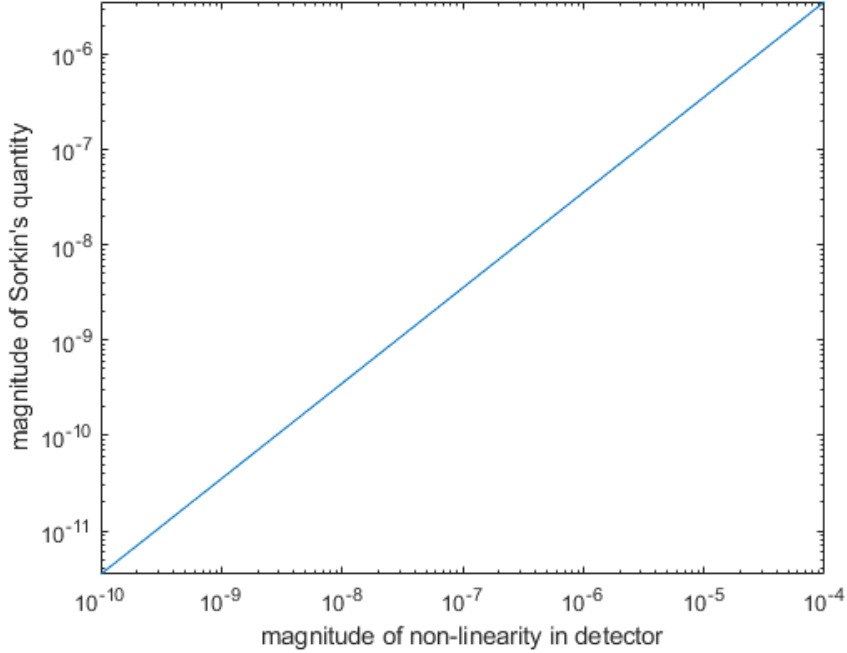
Figure 3.8: Sorkin's quantity for various strength of non-linearity in detector

the assumptions above. This can be useful to bound the error on Sorkin's quantity using detector's manufacturer specifications, or to determine non-linearities in the detection processes.

Since all linear processes do not produce higher-order interference (see Sec. 3.1), any non-zero higher-order interference detected in the form of Sorkin's quantity can be used to calculate the amount of non-linearity present in the detector. Experimental measurement of relation similar to Fig. 3.8 can be obtained using detectors with various known non-linearities and then interpolated. The relationship between presence and detection of non-linearity is summarized below:

presence of NL $\rightarrow$ presence of HOI $\rightarrow$ detection of HOI $\rightarrow$ detection of NL

3.4 Simulation of non-linear Schrödinger equation

We have discussed in Sec. 3.1 that all linear processes lead to $\mathcal{S}^3 = 0$. We want to explore the possibility of $\mathcal{S}^3 \neq 0$ using non-linear Schrödinger equations, such as Gross-Pitaevskii equation for Bose-Einstein condensate. The

non-linearity in these equations originates from the additional term compared to the usual Schrödinger equation:

$$i\hbar\frac{\partial\Psi}{\partial t} = -\frac{-\hbar^2}{2m}\nabla^2\Psi + V\Psi + \frac{4\pi\hbar^2 Na}{m}|\Psi|^2\Psi \qquad (3.22)$$

In particular, we apply Gross-Pitaevskii equation on a cloud of Lithium and Rubidium atoms, using parameters achieved experimentally [28, 34]. For convenience we reproduce the parameters here.

Quantity	Attractive condensate: Li	Repulsive condensate: Rb
m	$1.16 \times 10^{-26}\,kg$	$1.45 \times 10^{-25}\,kg$
a	-23.3 a_0	109 a_0
N	≤ 1400	100 000

Table 3.1: Parameters used to simulate experimentally achieved Bose-Einstein condensates. Bohr radius $a_0 = 0.529 \times 10^{-10}$. Adapted from [29].

We begin with cloud of atoms in coherent superposition of three Gaussians, each of $1\,\mu m$ wide, spatially separated by $5\,\mu m$. We evolve the system according to Gross-Pitaevskii equation for $1\,ms$ and calculate the corresponding Sorkin's quantity. Blocking is realised by removing the corresponding part of the initial superposition. The probabilities for part of superposition blocked are summarized in Fig. 3.9 and 3.10:
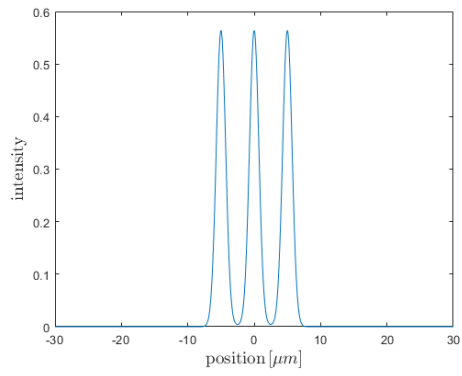
(a) Initial condition
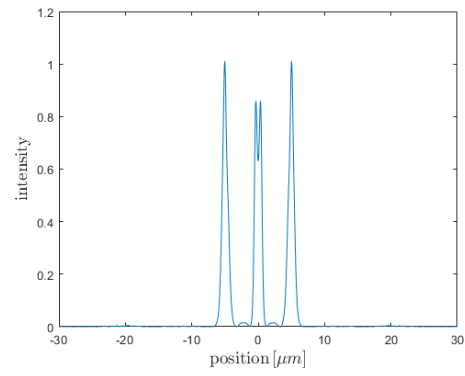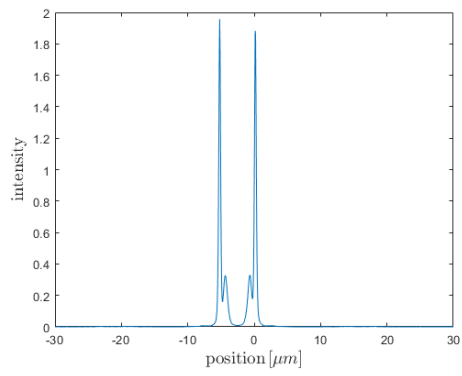
(b) All slits open I_{123}

(c) Slits 1,2 open I_{12}
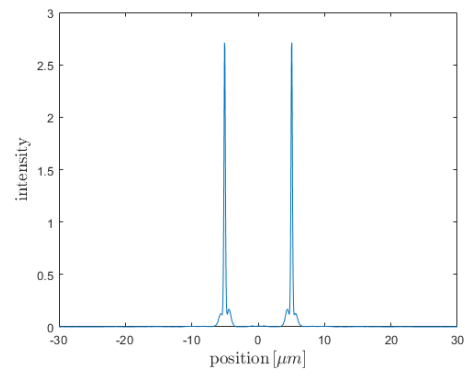
(d) Slits 1,3 open I_{13}
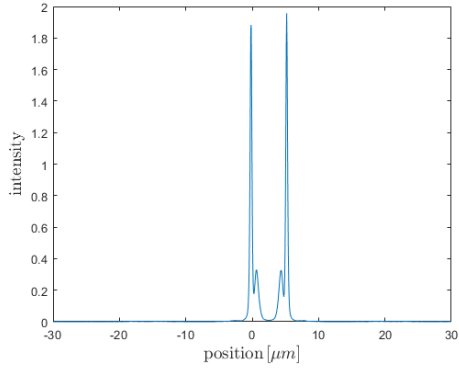
(e) Slits 2,3 open I_{23}
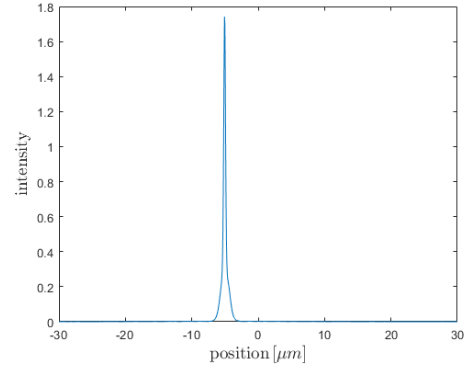
(f) Slit 1 open I_1
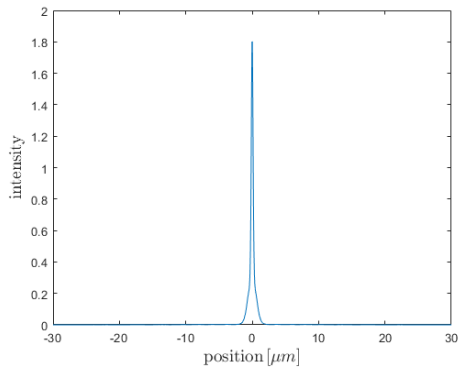
(g) Slit 2 open I_2
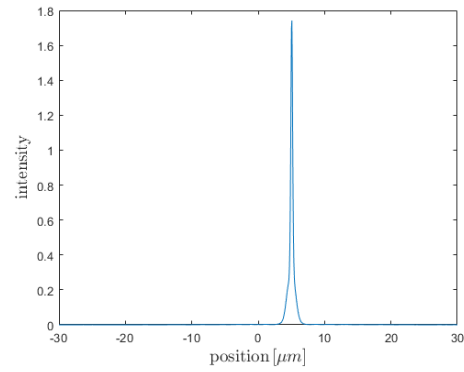
(h) Slit 3 open I_3

Figure 3.9: Intensities for Li atoms. Sorkin's quantity $\mathcal{S}^3$ is obtained by summing the intensities with signs according to Eq. 1.6.

For the condensate of Rubidium, we obtained the intensities below:
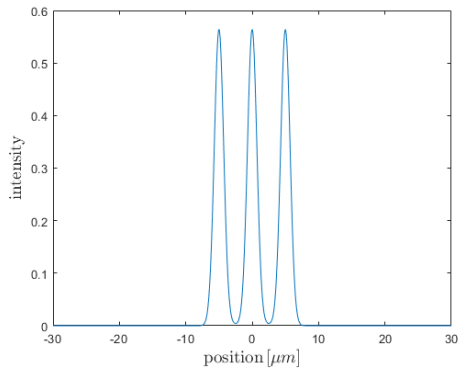
(a) Initial Condition
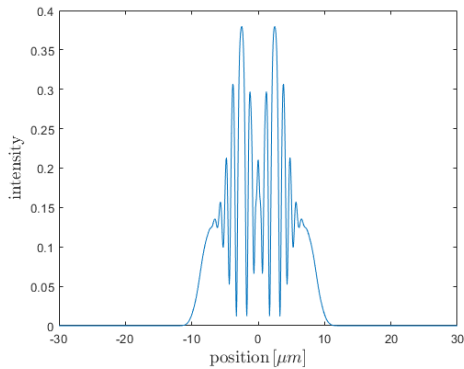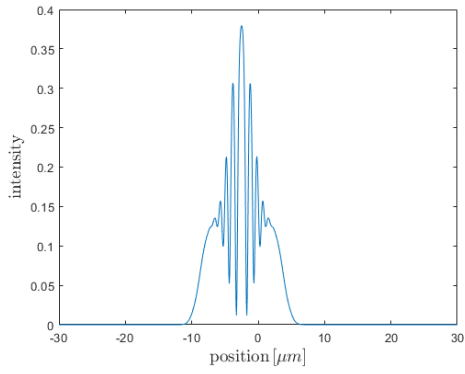
(b) All slits open I_{123}

(c) Slits 1,2 open I_{12}
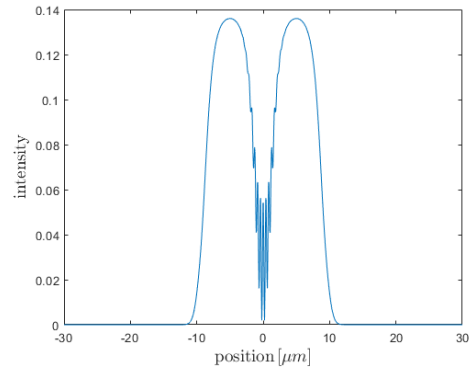
(d) Slits 1,3 open I_{13}
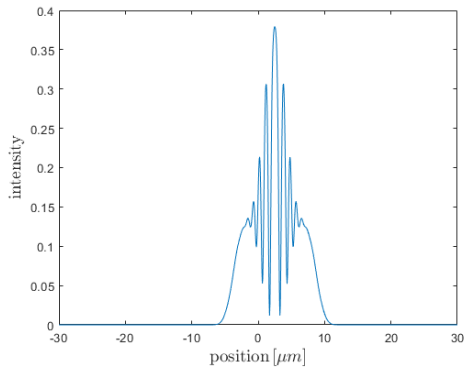
(e) Slits 2,3 open I_{23}
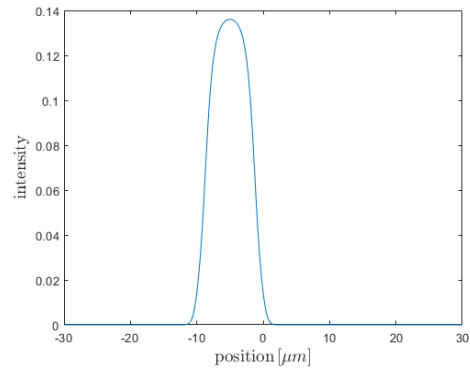
(f) Slit 1 open I_1
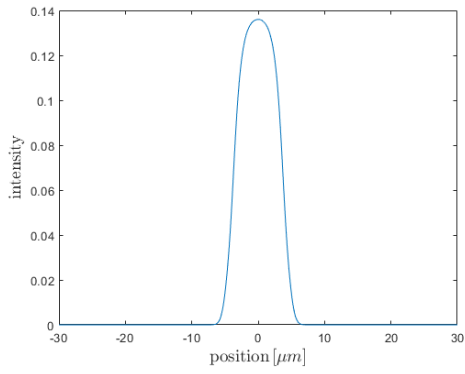
(g) Slit 2 open I_2
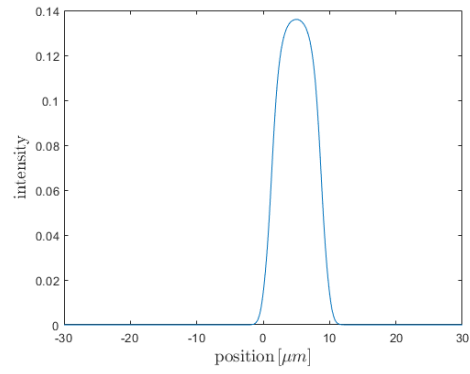
(h) Slit 3 open I_3

Figure 3.10: Intensities for Rb atoms. $\mathcal{S}^3$ is calculated in the same way as Li atoms.

The difference in behavior between the condensates can be attributed to their sign of scattering length a. When we compare the intensity plots in $a = 0$ Fig. 3.5(g) and $a < 0$ Fig. 3.9(g), we can see that for Li atoms, they attracts each other and make the peak narrower. As for Fig. 3.9(b), where we began with three spatially separated peaks, the evolved intensity is again three peaks, with less distance between the center of the peaks than the initial condition. Whereas for $a > 0$ Fig. 3.10(g), the Rb condensate repels itself and makes the peak wider than in Fig. 3.5(g). Hence in Fig. 3.10(b), the initial condition of three peaks evolves and becomes spatially jointed and create interference pattern.

The Sorkin's quantity for both species is plotted in Fig. 3.11 and showed clear signature of non-zero third order interference.
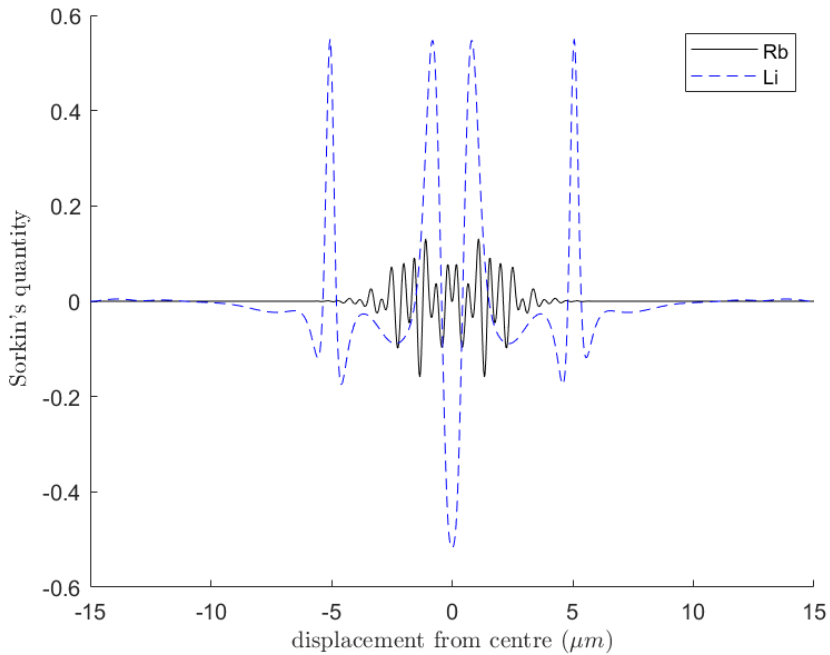
Figure 3.11: Sorkin's quantity $\mathcal{S}^3$ for Li and Rb atoms evolved with Gross-Pitaevskii equation

3.5 Summary

We derived conditions for higher-order interference to appear under the standard framework of second quantization. This requires presence of non-linear elements and indistinguishable particles. We theorized two methods for

producing higher-order interference, with non-linear optical media and non-linear Schrödinger equation. These methods can be applied to detect arbitrary order of interference if needed. We have also shown that non-linearity in the detection process leads to non-zero Sorkin's quantity $\mathcal{S}^3$. This may be used to characterise such non-linearities in the lab.

Chapter 4

Interference in post-quantum models [2]

Classically, we explore the physical world by directly interacting with it. We see by photons bouncing into eyes, smell by inhaling molecules into nose. Instruments merely extend our senses by interacting with the objects on our behalf. Quantum mechanics offers another possibility for enquiring whether an object is present at a given location — the interaction-free measurement [35]. It is possible by interferometric techniques to prepare a single quantum particle in superposition having one arm in a suspected location of the object and with the measurement scheme which, from time to time, identifies the presence of the object arguably without directly interacting with it [35–41]. We ask here if interaction-free measurements could be made perfect and provide non-trivial information about the presence of the object even if in each and every run the particle and the object to be detected do not interact directly. Within quantum formalism the answer is negative for which we provide an elementary argument as well as a quantitative relation covering this conclusion as a special case.

One could therefore say that we have identified yet another no-go theorem for quantum mechanics similar to no-cloning [42,43], no-broadcasting [44,45] or no-deleting [46]. Their importance comes from pinpointing special features of the quantum formalism (and nature) which can then be preserved or relaxed one by one when studying candidate physical theories. In the same spirit, we explore the possibility of perfect interaction-free measurements in the framework of density cubes [47] here. The basic idea behind this framework is to represent states by higher-rank tensors, density cubes, in direct analogy to quantum mechanical density matrices. In this way, more than

---

two classically exclusive possibilities can be coherently coupled giving rise to genuine multipath interference [7, 47]. The particular interferometer employed to theoretically demonstrate the multipath interference has a feature, also noted by Ref. [13], that the beam of particles used for detection is never found in one of the paths inside the interferometer but the presence of a detector in that path affects the final interference fringes. It is exactly this property that we shall exploit for the perfect interaction-free measurement. Therefore, within the density cubes model it becomes possible to identify the presence of an object without detecting any particles near the object. we consider this consequence too paradoxical to be realized in nature and hence a strong theoretical reason to reject the density cube model.

This chapter is organised as follows. In Sec. 4.1 we introduce interaction-free measurements and formally define perfect interaction-free measurement in a theory-independent way. We show that in all models where processes are assigned probability amplitudes, satisfying natural composition laws, there are no perfect interaction-free measurements and also no genuine multipath interference. Furthermore, we derive within quantum formalism a trade-off relation characterising interaction-free measurements, which explicitly shows the impossibility of such perfect measurements. We then move to the density cube model and gather in Sec. 4.2 all its elements necessary for our purposes. Similarly to the quantum case, we derive the trade-off relation within the density cube model, which now opens up the possibility of perfect interaction-free measurement. Subsec. 4.2.5 provides explicit examples of such measurements. The first example uses a three-path interferometer having the property that the particle is never found in the path where we place the detector, but the interaction-free measurement fails 50% of the time (we prove that this cannot be improved using the class of interferometers considered). In next example, we provide N-path interferometer giving rise to perfect interaction-free measurement and a vanishing probability of failure in the limit $N \to \infty$.

4.1 Interaction-free measurements

We begin with the original scheme by Elitzur and Vaidman [35]. The idea is presented and described in Fig. 4.1. The problem is famously dramatised by considering the presence or absence of a single-particle-sensitive bomb, the tradition we shall also follow.

For a general interferometer (with arbitrary number of paths and transformations replacing the balanced beam-splitters in Fig. 4.1) one always starts by tuning it to destructively interfere in at least one of its output ports.

In this way, if the click in one of these ports is observed we conclude that the bomb is present in the setup. This constitutes successful interaction-free measurement and we denote its probability by $P_!$. If the particle emerges in any other output port, we cannot make any definite statement as this happens both in the absence and presence of the bomb. The result is therefore inconclusive and we denote its probability by $P_?$. Finally, if the bomb is present, the probe particle triggers it with probability P_*. Clearly we have exhausted all possibilities and therefore

$$P_! + P_? + P_* = 1. \tag{4.1}$$
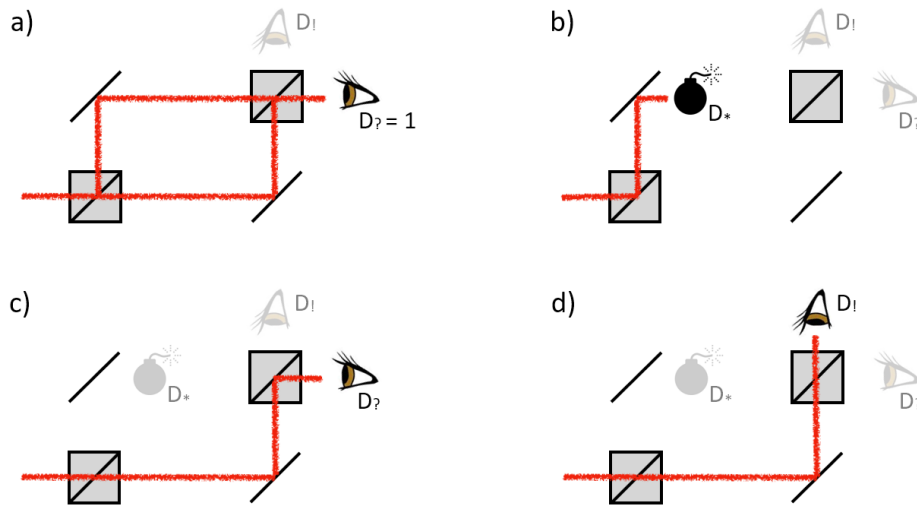
Figure 4.1: Interaction-free measurement and relevant parameters. Tuned Mach-Zehnder interferometer, as in panel a), is moved to the location where there might be a bomb in the upper arm. The probe particle triggers the bomb (single-particle-sensitive detector D_*) via path b) with probability P_*. The measurement is inconclusive if the particle takes path c) because detector labelled $D_?$ also fires when there is no bomb, see a). The probability of inconclusive result is denoted by $P_?$. Finally, the measurement succeeds if the top detector clicks and this happens with probability $P_!$, see d). The measurement is termed interaction-free because had the particle interacted with the bomb it would trigger it, and it did not.

4.1.1 Perfect interaction-free measurement

We call an interaction-free measurement perfect when statistics of single-shot experiments with the same interferometer shows

$$P_* = 0 \quad \text{and} \quad P_? < 1, \tag{4.2}$$

i.e. when bomb never explodes and yet from time to time we are certain it was there. We demonstrate an example where both of these probabilities are zero at the end of this chapter.

4.1.2 No perfect interaction-free measurements in amplitude models

In quantum mechanics, the condition $P_* = 0$ implies vanishing probability amplitude for the particle to propagate along the path of the bomb. This means that the first (generalised) beam-splitter never sends the particle to that path and hence it is irrelevant whether one places a bomb there or not, i.e. $P_? = 1$. The same conclusion holds in any theory that assigns probability amplitudes to physical processes and demands that vanishing probability of the process implies vanishing amplitude, e.g. probability is a power of the amplitude. It is intriguing in the present context that many of such models do not give rise to multipath interference. If the amplitudes are complex numbers (or even pairs of real numbers), their natural composition laws lead to Feynman rules, i.e. probability $\sim$ amplitude^2 [48, 49]. Sorkin's original argument then demonstrates absence of multipath interference.

Our definition of perfect interaction-free measurement, Eq. (4.2), demands $P_* = 0$ in every measurement run. In practice one might already be satisfied if P_* is small, so that in M experimental runs the bomb is unlikely to explode. Indeed such a setup exists and makes use of quantum Zeno effect in a looped interferometer [37]. The perfect interaction-free measurements we discuss in Subsec. 4.2.5 can also be looped and provide advantage over the quantum solution in the number of loops one has to execute in order to make $P_?$ small, say equal to ε. The best known quantum solution requires $M \sim 1/\varepsilon$ loops, whereas the post-quantum solution requires only $M = -\log \varepsilon$ and less loops, depending on the number of paths inside the interferometer. Having said this we focus our attention on single-shot experiments and derive now relation between P_* and $P_?$ within quantum formalism.

4.1.3 Quantum trade-off

Consider a general interferometer as shown in Fig. 4.2. We present the trade-off between P_* and $P_?$ for arbitrary mixed states but keeping the second transformation unitary, i.e. $\mathcal{T}_2 = \mathcal{U}_2$. Let us denote by ρ the density matrix of the particle inside the interferometer, right after the first transformation. The probability to trigger the bomb is given by

$$P_* = \langle 1| \rho |1\rangle. \tag{4.3}$$

If the bomb was not triggered state ρ gets updated to $\tilde{\rho}$ satisfying:

$$\tilde{\rho} = \frac{1}{1 - P_*}(\mathbb{1} - |1\rangle \langle 1|)\rho(\mathbb{1} - |1\rangle \langle 1|), \tag{4.4}$$

where $\mathbb{1}$ is the identity operator in the space of density matrices. Accordingly, the particle at the output of the interferometer is described by $\mathcal{U}_2 \tilde{\rho} \mathcal{U}_2^\dagger$. The probability of inconclusive result is given by the chance that now the particle is observed at those output ports $|s\rangle$ in which it might be present if there was no bomb:

$$P_? = (1 - P_*) \sum_s \langle s| \mathcal{U}_2 \tilde{\rho} \mathcal{U}_2^\dagger |s\rangle, \tag{4.5}$$

where we multiplied by $(1 - P_*)$ to account for the renormalisation in $\tilde{\rho}$. Let us denote the eigenstates of a density matrix ρ describing the particle inside the interferometer right after the first transformation as $|r\rangle$, i.e. $\rho = \sum_r p_r |r\rangle \langle r|$. We also write $\mathcal{U}_2 |r\rangle = |\phi_r\rangle$. From Eq. 4.5

$$\frac{P_?}{1 - P_*} = \mathrm{Tr}\left(\sum_s |s\rangle \langle s| \mathcal{U}_2 \tilde{\rho} \mathcal{U}_2^\dagger\right), \tag{4.6}$$

where the sum is over the paths $|s\rangle$ at the output of the interferometer where the particle could be found if there was no bomb, i.e. if $\mathcal{U}_2 \rho \mathcal{U}_2^\dagger = \sum_r p_r |\phi_r\rangle \langle \phi_r|$ is the state at the output. Therefore, states $|s\rangle$ span a subspace that contains the eigenstates $|\phi_r\rangle$ and we conclude

$$\sum_s |s\rangle \langle s| = \sum_r |\phi_r\rangle \langle \phi_r| + \sum_\mu |\mu\rangle \langle \mu|, \tag{4.7}$$

where $|\mu\rangle$'s complement the subspace spanned by the paths. Since $\langle \mu| \mathcal{U}_2 \tilde{\rho} \mathcal{U}_2^\dagger |\mu\rangle \geq 0$, Eq. (4.6) admits the lower bound:

$$\frac{P_?}{1 - P_*} \geq \mathrm{Tr}\left(\sum_r |\phi_r\rangle \langle \phi_r| \mathcal{U}_2 \tilde{\rho} \mathcal{U}_2^\dagger\right) = \mathrm{Tr}\left(\sum_r |r\rangle \langle r| \tilde{\rho}\right). \tag{4.8}$$

Using the definition of $\tilde{\rho}$ in terms of ρ given in Eq. 4.4

$$P_? \geq 1 - 2P_* + P_* \langle 1| E(\rho) |1\rangle$$
$$\geq (1 - P_*)^2, \tag{4.9}$$

where $E(\rho)$ is the projector on the support of ρ, i.e. $E(\rho) = \sum_r |r\rangle \langle r|$ for $\rho = \sum_r p_r |r\rangle \langle r|$. The last inequality in Eq. 4.9 follows from convexity, $\langle 1| E(\rho) |1\rangle \geq \langle 1| \rho |1\rangle$. We now discuss some special cases of this trade-off in order to illustrate tightness of the bound and for future comparison with the cubes model.
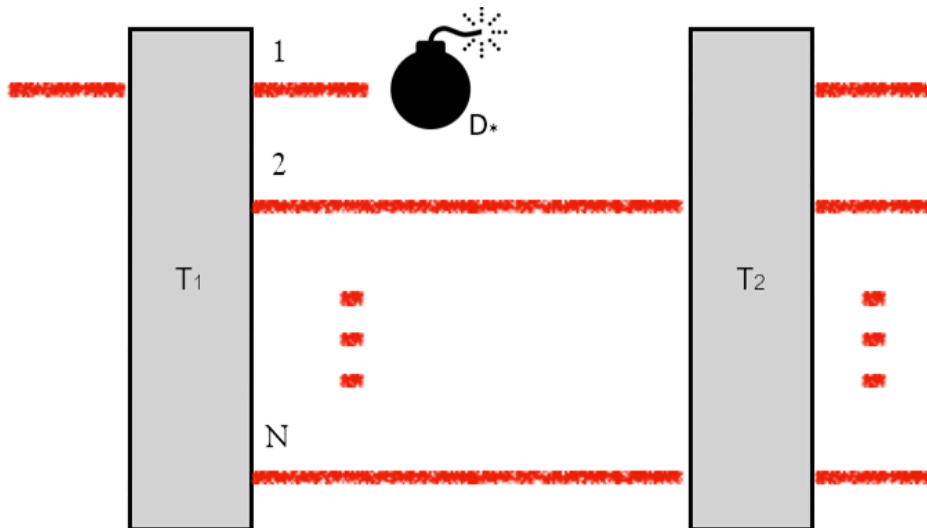
Figure 4.2: General interferometer used to derive the trade-off relations. The particle is injected into the first path. It then enters the interferometer via transformation $\mathcal{T}_1$ and leaves it via transformation $\mathcal{T}_2$. Inside the interferometer bomb is present in the first path.

First of all, due to convexity, the lower bound is saturated by pure states. In other words pure states are the best for interaction-free measurements. Note also that in quantum formalism by starting with a pure state ρ one always obtains a pure state $\tilde{\rho}$ after the measurement. It turns out that the cube model does not share this property and this could be seen as one of the reasons allowing a perfect interaction-free measurement.

Any density matrix ρ that does not contain coherence to the state $|1\rangle$ is useless for interaction-free measurements. If there is no coherence to state $|1\rangle$, then either (i) one of the eigenvectors of ρ is this state and the others are orthogonal to it or (ii) all the eigenvectors are orthogonal to $|1\rangle$. In the

case (i) we find $\langle 1| E(\rho) |1\rangle = 1$ and hence:

$$P_? = 1 - P_*. \tag{4.10}$$

The trade-off relation becomes an equality due to normalisation of the probabilities. Since both of the probabilities saturate the normalisation bound there is no place for a successful interaction-free measurement. In the case (ii) we note that $P_* = 0$ and hence the lower bound in Eq. 4.9 already shows that $P_? = 1$. This again demonstrates impossibility of perfect interaction-free measurements.

Finally, we note that the trade-off just derived holds for an arbitrary interferometer (with the second transformation being unitary) and is independent of the number of paths. For example, inequality 4.9 is saturated by taking the discrete Fourier transform as both transformations in the interferometer involving an arbitrary number of paths. This again will be different in the density cube model.

4.2   Density cubes

The trade-off relation just derived captures the impossibility of perfect interaction-free measurement in the quantum formalism. We show here that their absence is a natural postulate which disqualifies certain extensions of quantum mechanics, namely, the density cube model [47]. This model has been introduced in order to incorporate the possibility of multipath coherence. Why does quantum mechanics "stop" at second-order interference? How would a model that gives rise to third-order and higher-order interference look? The density cube formalism provides the answer to the latter question. In principle it could show up in triple-slit experiments. However, we find that this is unlikely because density cubes allow for perfect interaction-free measurements. We first introduce the elements of the cubes model. Then derivation the trade-off relation between $P_?$ and P_* within the density cubes framework will be done, which hints at the possibility of perfect interaction-free measurement. Finally, we provide explicit examples of such measurements.

4.2.1   Probability

The basic entity of the model is a density cube C: a rank-3 tensor with complex elements $C_{jkl} \in \mathbb{C}$. The density cubes are assumed to be Hermitian in a sense that exchanging any two indices produces a complex conjugated element, e.g.:

$$C_{jkl} = C_{kjl}^* = C_{klj} \tag{4.11}$$

Hermitian cubes form a real vector space with inner product

$$(M, C) = \sum_{j,k,l=1}^{N} M_{jkl}^* C_{jkl}, \tag{4.12}$$

where each index of the tensor runs through values $1, \ldots, N$. Therefore, one naturally defines the probability to observe outcome corresponding to cube M in a measurement on a physical object described by cube C by the above inner product. This is in close analogy to the Born rule in quantum mechanics which in the same situation assigns probability $\mathrm{Tr}(MC) = \sum_{j,k=1}^{N} M_{jk}^* C_{jk}$, with M and C being density matrices. In this way the model of density cubes extends self-duality between states and measurements present in quantum mechanics [50, 51].

4.2.2 States

We shall consider two types of density cubes: the quantum cubes which represent quantum states in the density cube model and non-quantum cubes (with triple-path coherence) which extend the quantum set. The former are constructed from quantum states and are in one-to-one relation with the quantum states. While non-quantum cubes are also constructed starting from a quantum state, one can choose various combinations for the triple-path coherence terms to construct several distinct non-quantum cubes corresponding to a given quantum state.

Quantum cubes

Consider the following mapping between a density matrix ρ and a cube C^Q:

$$
\begin{aligned}
C_{jjj}^Q &= \rho_{jj}, \\
C_{jjk}^Q &= \sqrt{\tfrac{2}{3}}\,\mathrm{Re}(\rho_{jk}), &\text{for}\quad j < k, \\
C_{jkk}^Q &= \sqrt{\tfrac{2}{3}}\,\mathrm{Im}(\rho_{jk}), &\text{for}\quad j < k, \\
C_{jkl}^Q &= 0, &\text{for}\quad j \neq k \neq l.
\end{aligned}
\tag{4.13}
$$

Note that all the terms C_{jkl}^Q where the three indices are different are set to zero, meaning that these cubes do not admit any three-path coherence. The remaining elements can be computed using the Hermiticity rule. This mapping preserves the inner product between the states and hence quantum mechanics and density cube model with this set of cubes are physically

equivalent. For example, the inner product of an arbitrary 2-level state with itself, i.e. $\langle C^Q | C^Q \rangle = 1$, we expect density cube solution to be identical.

$$C = \left\{ \begin{pmatrix} C_{111} & C_{112} \\ C_{121} & C_{122} \end{pmatrix}, \begin{pmatrix} C_{211} & C_{212} \\ C_{221} & C_{222} \end{pmatrix} \right\}$$

$$C^Q = \begin{pmatrix} C_{11} & C_{12} \\ C_{21} & C_{22} \end{pmatrix} \tag{4.14a}$$

$$(C, C) = C_{111}^2 + C_{222}^2 + C_{112}^2 + C_{121}^2 + C_{122}^2 + C_{211}^2 + C_{212}^2 + C_{221}^2$$

$$= C_{11}^2 + C_{22}^2 + \frac{2}{3}(\mathrm{Re}(C_{12}))^2 + \frac{2}{3}(\mathrm{Re}(C_{12}))^2 + \frac{2}{3}(\mathrm{Im}(C_{12}))^2$$

$$+ \frac{2}{3}(\mathrm{Re}(C_{12}))^2 + \frac{2}{3}(\mathrm{Im}(C_{12}))^2 + \frac{2}{3}(\mathrm{Im}(C_{12}))^2$$

$$= C_{11}^2 + C_{22}^2 + 2(\mathrm{Re}(C_{12}))^2 + 2(\mathrm{Im}(C_{12}))^2 \tag{4.14b}$$

$$= \langle C^Q | C^Q \rangle = 1 \tag{4.14c}$$

Non-quantum cubes

We now extend the set of quantum cubes and allow for non-trivial triple-path coherence by mapping every quantum state ρ to the following family of cubes:

$$\begin{aligned}
C_{jjj} &= \frac{1}{N-1}(1 - \rho_{jj}), \\
C_{jjk} &= \sqrt{\frac{2}{3}} \frac{1}{N-1} \mathrm{Re}(\rho_{jk}), \quad \text{for} \quad j < k, \\
C_{jkk} &= \sqrt{\frac{2}{3}} \frac{1}{N-1} \mathrm{Im}(\rho_{jk}), \quad \text{for} \quad j < k, \\
C_{1jk}(\gamma) &= \sqrt{\frac{1}{3}} \frac{1}{N-1} \omega^{f(\gamma,j,k)}, \quad \text{for} \quad 1 < j < k,
\end{aligned} \tag{4.15}$$

where $\omega = \exp(-i2\pi/N)$ is the Nth complex root of unity and $f(\gamma, j, k) = \{1, \dots, N\}$. Parameter $\gamma = 1, \dots, N$ enumerates different cubes that can be constructed from a given quantum state. Again, the remaining elements can be completed using the Hermiticity rule. We provide explicit examples of interesting non-quantum cubes in section 4.2.5 and Appendix B.1. Note that for simplicity we choose to place the bomb in the first path of the interferometer and therefore we consider cubes where the three-path coherence involves only state 1 (the first path) and two other states. All the terms C_{jkl}, with three different indices, each of which is strictly greater than 1, are set to zero.

It is convenient to distinguish a *quantum part* of the non-quantum cube. The quantum part $Q(C)$ is obtained by applying isomorphism in Eq. 4.13 to cube C assuming its three-path coherences vanish. One immediately finds:

$$Q(C) = \frac{1}{N-1}(\mathbb{1} - \rho), \tag{4.16}$$

where $\mathbb{1}$ denotes $N \times N$ identity matrix. The probability rule now splits into the quantum part and the part depending only on the three-path coherences:

$$(M, C) = \mathrm{Tr}[Q(M)Q(C)] + \sum_{j \neq k \neq l} M_{jkl}^*(\gamma')C_{jkl}(\gamma), \tag{4.17}$$

where γ' and γ specify the cubes M and C according to Eq. 4.15. It is now clear that non-quantum cubes have non-negative overlap with all the quantum cubes, as it should be for a probability, because the latter do not give rise to three-path coherence. We still have to ensure that the inner products between all the non-quantum cubes are non-negative and bounded by one. The set of non-quantum cubes of interest here will be shown to be finite and satisfying this requirement.

4.2.3 Measurement

We shall only be interested in enquiring about particle's path at various stages of the evolution. Furthermore, we will focus on checking whether the particle is in the first path or not. Clearly this measurement is allowed in quantum mechanics and we choose standard basis as the basis of which-path measurement. The corresponding quantum cube looks as follows in the case of triple-path experiment:

$$M_1 = \left\{ \begin{pmatrix} 1 & 0 & 0 \\ 0 & 0 & 0 \\ 0 & 0 & 0 \end{pmatrix}, \begin{pmatrix} 0 & 0 & 0 \\ 0 & 0 & 0 \\ 0 & 0 & 0 \end{pmatrix}, \begin{pmatrix} 0 & 0 & 0 \\ 0 & 0 & 0 \\ 0 & 0 & 0 \end{pmatrix} \right\}, \tag{4.18}$$

where the three 3×3 matrices describe the cube with elements C_{1jk}, C_{2jk} and C_{3jk}, respectively. The probability that a particle described by cube C is found in the first path is (M_1, C).

It is essential to the interaction-free measurement to describe the state of the particle after it has *not* been found in a particular path. Here the model of density cubes also follows quantum mechanics and it is assumed that the cube describing the system changes as a result of measurement. If the particle is found in the nth path its state gets updated $C \to M_n$, where M_n is the

quantum cube corresponding to a particle propagating along the nth path. If the particle is not found in the nth path the model follows generalised Lüder's state update rule: erases from the cube all elements C_{jkl} with $j, k, l = n$, and renormalises the remaining elements. Following our three-path example, if the particle is not found in the first path its generic cube C gets updated to:

$$
\tilde{C} = \left\{ \begin{pmatrix} 0 & 0 & 0 \\ 0 & 0 & 0 \\ 0 & 0 & 0 \end{pmatrix}, \begin{pmatrix} 0 & 0 & 0 \\ 0 & \tilde{C}_{222} & \tilde{C}_{223} \\ 0 & \tilde{C}_{232} & \tilde{C}_{233} \end{pmatrix}, \begin{pmatrix} 0 & 0 & 0 \\ 0 & \tilde{C}_{322} & \tilde{C}_{323} \\ 0 & \tilde{C}_{332} & \tilde{C}_{333} \end{pmatrix} \right\},
$$

(4.19)

where

$$
\tilde{C}_{jkl} = \frac{1}{1 - C_{111}} C_{jkl},
$$

(4.20)

is the cube element renormalised by the probability that the particle is not in the first path.

At this stage it has to be ensured that all post-measurement cubes are allowed within the model. This is immediately clear if one begins with a quantum cube. For the non-quantum cubes we note that we only consider those cubes which have three-path coherence to the first path and we only enquire whether the particle is in the first path or not. If the measurement does not find the particle in the first path all these coherences are updated to zero and accordingly the post-measurement cube is a quantum one.

4.2.4   Cubes trade-off

We are now ready to present the trade-off relation between P_* and $P_?$ for a general interferometer in Fig. 4.2. Our trade-off relation holds for transformation $\mathcal{T}_2$ that preserves the inner product, while having an additional assumption on the structure of cube C describing the particle inside the interferometer right after $\mathcal{T}_1$. We assume that after the particle has propagated through the whole interferometer in the case of no bomb, the cube at the output does not have any two-path and three-path coherence:

$$
\mathcal{T}_2(C) = \sum_s p_s M_s.
$$

(4.21)

We ensure this is always fulfilled in our examples. Similarly to the quantum case, the probabilities entering the trade-off are defined as follows:

$$P_* = (M_1, C)$$

$$P_? = (1 - P_*) \sum_s (M_s, \mathcal{T}_2(\tilde{C})) \tag{4.22}$$

$$\tag{4.23}$$

Therefore:

$$\frac{P_?}{1 - P_*} = \sum_s (M_s, \mathcal{T}_2(\tilde{C}))$$

$$\geq \sum_s (p_s M_s, \mathcal{T}_2(\tilde{C}))$$

$$= (\mathcal{T}_2(C), \mathcal{T}_2(\tilde{C})) = (C, \tilde{C}) \tag{4.24}$$

where the cube $\tilde{C}$ represents the particle inside the interferometer after the measurement in the first path has not found the particle there, see Eq. 4.19. The inequality follows from convexity, then we used Eq. 4.21 and finally the fact that $\mathcal{T}_2$ preserves the inner product. Next, we shall find the minimum of the right-hand side. Using the expression for the elements of $\tilde{C}$ in terms of elements of C we find:

$$(C, \tilde{C}) = \frac{1}{1 - P_*} \sum_{j,k,l=2}^{N} |C_{jkl}|^2, \tag{4.25}$$

where $C_{222} + \cdots + C_{NNN} = 1 - P_*$. Since all of the summands are non-negative we get the lower bound by setting all the off-diagonal terms to zero. It is then easy to verify that the minimum is achieved for even distribution of the probability:

$$C_{nnn} = \frac{1 - P_*}{N - 1} \quad \text{for } n = 2, \dots, N. \tag{4.26}$$

Using this lower bound in (4.24) we obtain:

$$P_? \geq \frac{(1 - P_*)^2}{N - 1}. \tag{4.27}$$

It is illustrated in Fig. 4.3. One recognises that for $N = 2$ this relation reduces to the one derived in quantum mechanics. For two-path interferometers this is not surprising as in this case the density cube model reduces to standard

quantum formalism [47]. For higher number of paths, this relation emphasises that independence of the number of paths is a special quantum feature.
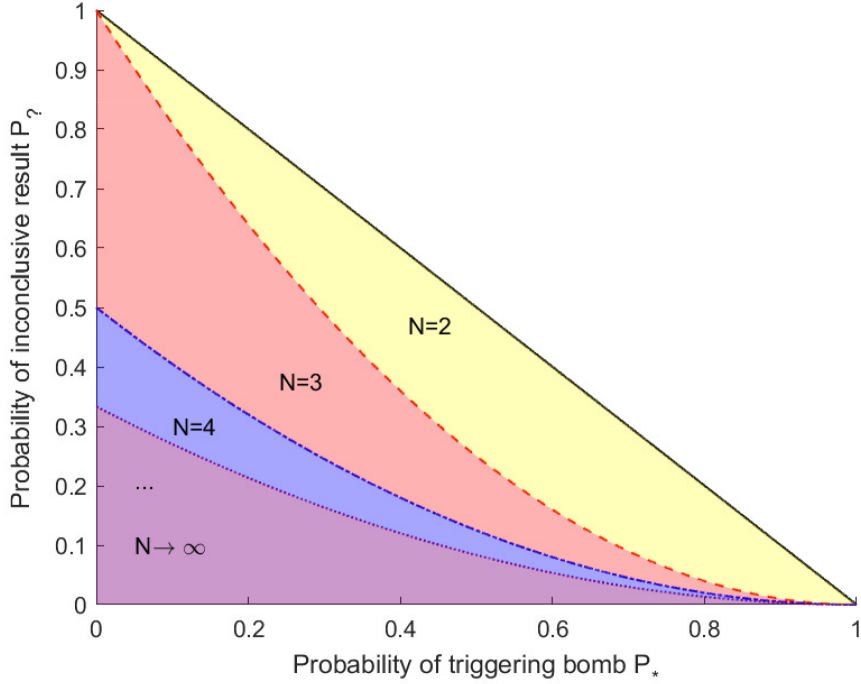
Figure 4.3: Trade-off between the probability to trigger the bomb, P_*, and the probability of inconclusive result, $P_?$, within the cubes model and quantum mechanics. The straight line illustrates the trivial bound $P_* + P_? = 1$. All other region borders give lower bounds on the value of $P_?$ as a function of P_*. The allowed region for N' number of paths inside the interferometer contains also the regions of N, where $N' > N$. The quantum mechanical trade-off coincides with the case of $N = 2$. Perfect interaction-free measurements can occur if the allowed values on the vertical axis are less than 1, i.e. $P_* = 0$ and $P_? < 1$ simultaneously.

Relation 4.27 opens up a possibility of perfect interaction-free measurements. Indeed for all $N \geq 3$ one finds that the right-hand side of the equation is strictly less than 1 even if $P_* = 0$. Furthermore, both probabilities P_* and $P_?$ can in principle be brought to zero in the limit $N \to \infty$. This can be achieved by setting only a single detector in path 1 in Fig. 4.2 to represent inconclusive result, and all the other detectors to represent conclusive detection, which saturates the lower bound set by the trade-off relation 4.27. In the next section we provide such explicit examples.

4.2.5 Examples of perfect interaction-free measurements

We present in detail the workings of the perfect interaction-free measurement in the case of three-path interferometer with emphasis on the features departing from quantum formalism. We will then generalize to N paths.

Three paths

Consider the setup described in Fig. 4.4. The transformation $\mathcal{T}_1 = \mathcal{T}_2 = \mathcal{T} \circ \mathcal{D}$ is chosen to consist of (quantum mechanical) complete dephasing of two-path coherences, $\mathcal{D}$, followed by the transformation $\mathcal{T}$ defined in Eq. 16 of Ref. [47], which we will review here for completeness. In addition, we require $\mathcal{T}$ to be an involution, i.e. $\mathcal{T}^2 = \mathbb{1}$. The reason behind this composition of operations is that $\mathcal{T}$ is only defined on a subset of cubes and it might be that it is impossible to extend it consistently to the whole set of cubes. The role of the dephasing is then to bring an arbitrary cube to the subset on which $\mathcal{T}$ is known to act consistently. The dephasing operation is defined
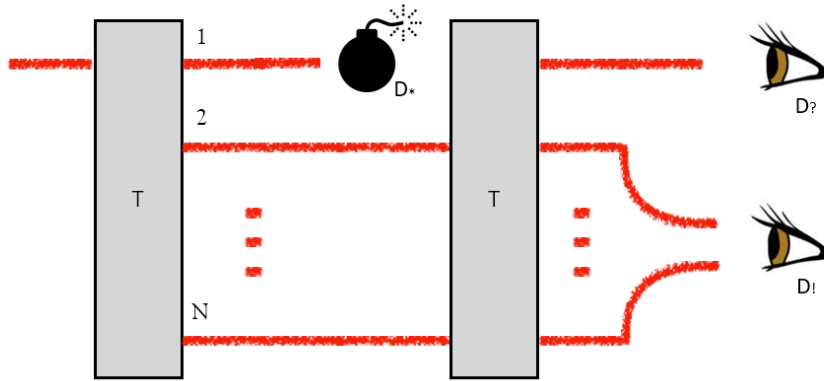
Figure 4.4: Schematics for perfect interaction-free measurement experiment within the density cube model. The cube describing the particle inside the interferometer has only triple-path coherences to the first path and yet vanishing element C_{111}. Therefore the particle is never found along the first path inside the interferometer and the bomb never detonates, $P_* = 0$. But the presence of the bomb removes the triple-path coherences from the cube and alters the state, which allows us to detect the bomb.

to remove completely all two-path coherences in a cube and leave unaffected the diagonal elements C_{nnn} and triple-path coherences C_{jkl} with all indices different. Since this operation acts only on the quantum part of the cube it produces allowed cubes. Transformation $\mathcal{T}$ has matrix representation

$$
\mathcal{T} = \frac{1}{2} \begin{pmatrix} 0 & 1 & 1 & 1 & 1 \\ 1 & 0 & 1 & \omega^* & \omega \\ 1 & 1 & 0 & \omega & \omega^* \\ 1 & \omega & \omega^* & 1 & 0 \\ 1 & \omega^* & \omega & 0 & 1 \end{pmatrix}, \tag{4.28}
$$

when written in the following sub-basis of Hermitian cubes:

$$
\begin{aligned}
B_1 &= M_1, \qquad B_2 = M_2, \qquad B_3 = M_3, \\
B_4 &= \frac{1}{\sqrt{3}} \left\{ \begin{pmatrix} 0 & 0 & 0 \\ 0 & 0 & 1 \\ 0 & 0 & 0 \end{pmatrix}, \begin{pmatrix} 0 & 0 & 0 \\ 0 & 0 & 0 \\ 1 & 0 & 0 \end{pmatrix}, \begin{pmatrix} 0 & 1 & 0 \\ 0 & 0 & 0 \\ 0 & 0 & 0 \end{pmatrix} \right\}, \\
B_5 &= \frac{1}{\sqrt{3}} \left\{ \begin{pmatrix} 0 & 0 & 0 \\ 0 & 0 & 0 \\ 0 & 1 & 0 \end{pmatrix}, \begin{pmatrix} 0 & 0 & 1 \\ 0 & 0 & 0 \\ 0 & 0 & 0 \end{pmatrix}, \begin{pmatrix} 0 & 0 & 0 \\ 1 & 0 & 0 \\ 0 & 0 & 0 \end{pmatrix} \right\}.
\end{aligned} \tag{4.29}
$$

That is, given an arbitrary cube C in this subspace, the transformation $\mathcal{T}$ acts upon it via ordinary matrix multiplication on the vector representation of C, i.e. a five-dimensional column vector with jth component given by (C, B_j). As already alluded to, this subspace consists of cubes which have no two-path coherences, but solely three-path coherences and the diagonal terms. It is now straightforward to verify that $\mathcal{T}$ is an involution in the considered subspace. Accordingly, if the particle enters the interferometer without the bomb though the first path, it is always found in the first output port of the setup. This adheres to our assumption in Eq. 4.21 as the output cube is simply M_1.

Transformation $\mathcal{T}$ is different from arbitrary unitary transformation as it produces triple-path coherence inside the interferometer. The particle injected into the first path is described by the cube M_1, which in the considered subspace corresponds to the vector $[1\,0\,0\,0\,0]^T$ and one can verify that the corresponding cube after application of $\mathcal{T}$ is $\mathcal{T}(M_1) = \frac{1}{2}(B_2 + B_3 + B_4 + B_5) = C$, which in cube form is given by:

$$
C = \frac{1}{2} \left\{ \begin{pmatrix} 0 & 0 & 0 \\ 0 & 0 & \frac{1}{\sqrt{3}} \\ 0 & \frac{1}{\sqrt{3}} & 0 \end{pmatrix}, \begin{pmatrix} 0 & 0 & \frac{1}{\sqrt{3}} \\ 0 & 1 & 0 \\ \frac{1}{\sqrt{3}} & 0 & 0 \end{pmatrix}, \begin{pmatrix} 0 & \frac{1}{\sqrt{3}} & 0 \\ \frac{1}{\sqrt{3}} & 0 & 0 \\ 0 & 0 & 1 \end{pmatrix} \right\}. \tag{4.30}
$$

Note that it is a pure cube, i.e. $(C, C) = 1$, and it contains solely three-path coherences and elements C_{222} and C_{333}. The essential feature we are utilising for perfect interaction-free measurement is the presence of these coherences even though the probability to find the particle in the first path vanishes

$$P_* = (M_1, C) = 0. \tag{4.31}$$

A similar statement for quantum states does not hold. If the probability to locate a quantum particle in the first path vanishes, all coherences to this path must vanish, as otherwise the corresponding density matrix has negative eigenvalues.

If the bomb is present inside the interferometer but it is not triggered the state update rule dictates to erase all elements C_{jkl} with any of $j, k, l = 1$. We obtain the following cube:

$$\tilde{C} = \left\{ \begin{pmatrix} 0 & 0 & 0 \\ 0 & 0 & 0 \\ 0 & 0 & 0 \end{pmatrix}, \begin{pmatrix} 0 & 0 & 0 \\ 0 & \frac{1}{2} & 0 \\ 0 & 0 & 0 \end{pmatrix}, \begin{pmatrix} 0 & 0 & 0 \\ 0 & 0 & 0 \\ 0 & 0 & \frac{1}{2} \end{pmatrix} \right\}. \tag{4.32}$$

It contains no coherences whatsoever and it is mixed, i.e. $(\tilde{C}, \tilde{C}) = \frac{1}{2}$. We started with a pure cube and post-selected a mixed one. This is also not allowed within quantum formalism, where any pure state $|\psi\rangle = \sum_{n=1}^{N} \alpha_n |n\rangle$ gets updated to another pure state $|\tilde{\psi}\rangle = \sum_{n=2}^{N} \tilde{\alpha}_n |n\rangle$, with $\tilde{\alpha}_n = \alpha_n / \sqrt{1 - |\alpha_1|^2}$. Finally, we evolve $\tilde{C} = \frac{1}{2} M_2 + \frac{1}{2} M_3$ through the second transformation and find that $\mathcal{T}(\tilde{C})$ is given by (dephasing has no effect here):

$$\frac{1}{4} \left\{ \begin{pmatrix} 2 & 0 & 0 \\ 0 & 0 & -\frac{1}{\sqrt{3}} \\ 0 & -\frac{1}{\sqrt{3}} & 0 \end{pmatrix}, \begin{pmatrix} 0 & 0 & -\frac{1}{\sqrt{3}} \\ 0 & 1 & 0 \\ -\frac{1}{\sqrt{3}} & 0 & 0 \end{pmatrix}, \begin{pmatrix} 0 & -\frac{1}{\sqrt{3}} & 0 \\ -\frac{1}{\sqrt{3}} & 0 & 0 \\ 0 & 0 & 1 \end{pmatrix} \right\}.$$

The probability of inconclusive result is given by the probability that the particle is found in the first path, as it was always there in the absence of the bomb, and therefore we find:

$$P_? = (M_1, \mathcal{T}(\tilde{C})) = \frac{1}{2}. \tag{4.33}$$

This probability saturates the lower bound derived in Eq. 4.27 for $N = 3$ and hence the setup discussed is optimal. The probability of successful measurement is therefore

$$P_! = 1 - P_* - P_? = 1 - 0 - \frac{1}{2} = \frac{1}{2} \tag{4.34}$$

More than three paths

We now generalise above scheme to more than three paths and show that the density cube model allows for perfect interaction-free measurement which in every run provides complete information about the presence of the bomb. However, this only holds in the limit $N \to \infty$.

We shall now construct a set of N pure orthonormal cubes, $C^{(n)}$, which will then be used to provide transformation $\mathcal{T}$ of the optimal interferometer, i.e. giving rise to the minimal probability of inconclusive result while keeping $P_* = 0$. We set the modulus of all the three-path coherences within each cube $C^{(n)}$ to be the same and choose its non-zero elements as follows:

$$C_{jjj}^{(n)} = \frac{1}{N-1}, \qquad \text{for } j \neq n, \tag{4.35a}$$

$$C_{1jk}^{(n)} = \sqrt{\frac{1}{3}} \frac{1}{N-1} \, x_{jk}^{(n)}, \quad \text{for } 1 < j < k. \tag{4.35b}$$

The other non-zero elements can be found from the Hermiticity rule. In this way, the three-path coherences in cube $C^{(n)}$ are represented by a set of phases $x_{jk}^{(n)}$, which are unknown at the moment. We arrange the independent phases, i.e. the ones having $j < k$, into a vector $\vec{x}_n$. The orthonormality conditions between the cubes are now expressed in the following equations

$$(C^{(n)}, C^{(n)}) = 1 \iff |(\vec{x}_n)_l| = 1$$
$$\text{for all } n, l, \tag{4.36a}$$

$$(C^{(m)}, C^{(n)}) = 0 \iff (\vec{x}_m, \vec{x}_n) + (\vec{x}_n, \vec{x}_m) = 2 - N,$$
$$\text{for all } m \neq n. \tag{4.36b}$$

where $(\vec{x}_n)_l$ is the lth component of vector $\vec{x}_n$. Equations (4.36) are solved in Appendix B.1. Let us write the solution in form of a matrix

$$X = (\vec{x}_1 \ldots \vec{x}_N), \tag{4.37}$$

having vectors $\vec{x}_n$ as columns. We now show how to use it to construct the "cube multiport" transformation $\mathcal{T}$.

We assume the two transformations in the setup are the same and that $\mathcal{T}$ is defined solely on the subspace of Hermitian cubes which do not have any two-path coherences. The cubes forming the basis set for this subspace are

as follows:

$$B^{(n)}_{jkl} = \delta_{jn}\delta_{kn}\delta_{ln}, \tag{4.38a}$$

for $n = 1, \ldots, N$

$$B^{(vw)}_{jkl} = \frac{1}{\sqrt{3}} \left(\delta_{j1}\delta_{kv}\delta_{lw} + \delta_{jw}\delta_{k1}\delta_{lv} + \delta_{jv}\delta_{kw}\delta_{l1} \right), \tag{4.38b}$$

for $1 < v < w \leq N$,

$$B^{(wv)}_{jkl} = \frac{1}{\sqrt{3}} \left(\delta_{j1}\delta_{kw}\delta_{lv} + \delta_{jv}\delta_{k1}\delta_{lw} + \delta_{jw}\delta_{kv}\delta_{l1} \right), \tag{4.38c}$$

for $1 < v < w \leq N$.

One recognises that the cubes in the first line are just the M_n cubes describing the particle propagating along the nth path. The cubes in the second line describe independent three-path coherences, and the cubes in the third line their complex conjugations. Altogether there are $d = N + (N-1)(N-2)$ cubes in this sub-basis and transformation $\mathcal{T}$ is represented by $d \times d$ matrix. We divide $\mathcal{T}$ into four blocks:

$$\mathcal{T} = \left(\begin{array}{c|c} A & C \\ \hline B & D \end{array} \right), \tag{4.39}$$

A being a square $N \times N$ matrix, D being a square matrix with dimension $(N-1)(N-2) \times (N-1)(N-2)$, and B and C being rectangular. By imposing that $\mathcal{T}(M_n) = C^{(n)}$ matrices A and B are fixed to

$$A = \frac{1}{N-1} \begin{pmatrix} 0 & 1 & \cdots & 1 \\ 1 & 0 & \cdots & 1 \\ \vdots & \vdots & \ddots & \vdots \\ 1 & 1 & \cdots & 0 \end{pmatrix}, \qquad B = \begin{pmatrix} X \\ X^* \end{pmatrix}. \tag{4.40}$$

By further requiring involution $\mathcal{T}^2 = \mathbb{1}$ and Hermiticity $\mathcal{T} = \mathcal{T}^\dagger$ one finds that

$$C = B^\dagger, \qquad D = \sqrt{\mathbb{1} - BB^\dagger}. \tag{4.41}$$

We show in Appendix B.3 that $\mathbb{1} - BB^\dagger$ is indeed a positive matrix, which implied that it is invertible and applicable to be solved by Schur compliment method. This concludes our construction of $\mathcal{T}$. It turns out that this is not the only way to construct the cube multiport transformation and we provide other examples in the Appendix B.3. All of them transform the quantum cubes M_n to the non-quantum cubes $C^{(n)}$. Note that in the considered subspace M_n are the only pure quantum cubes and one verifies that $C^{(n)}$ are the only pure non-quantum cubes allowed. In this way $\mathcal{T}$ is shown to act consistently, i.e. map cubes allowed within the model to other allowed cubes.

4.3   Summary

We proposed a theory-independent definition of perfect interaction-free measurement. It turns out that quantum mechanics does not allow this possibility but it can be realised within the framework of density cubes [47]. Notably, this framework allows transformations that prepare triple-path coherence involving a path where the probability of detecting the particle is strictly zero. Nevertheless, this coherence can be destroyed if the bomb (detector) is in the setup, leading to a distinguishable outcome in a suitable one-shot interference experiment.[3] We therefore propose that such operations should not be present in a physical theory as they effectively allow deduction of the presence of an object in a particular location without ever interacting with the said object. This might be considered as a natural postulate about physical theories or one might also try to identify other more basic postulates which imply impossibility of perfect interaction-free measurements.

In this context we note that perfect interaction-free measurements are consistent with the no-signalling principle (no super-luminar communication). In the density cube model it is the triple-path coherence that is being destroyed by the presence of the detector inside the interferometer. The statistics of any observable measured on the remaining paths is the same independently of whether the detector is in the setup or not. Hence the information about its presence can only be acquired after recombining the paths together, which can be done at most with the speed of light. The situation resembles that of the stronger than quantum correlations satisfying the principle of no-signalling [52]. They are considered "too strong" as they trivialise communication complexity [53, 54] or random access coding [55], and they are at variance with many natural postulates [55–57]. Similarly, we consider identifying presence of a detector without ever triggering it, i.e. a perfect interaction-free measurement, as too powerful to be realised in nature. Exactly which physical principles forbid such measurements is, of course, an interesting question.

---

[3]We emphasise that here we study single-shot experiments in contrast to quantum Zeno effect which allows for perfect interaction-free measurements in the limit of infinitely many uses of the interferometer [37].

Chapter 5

Conclusions

We introduced the concept of "genuine multi-path interference" and tools to quantify it, such as Sorkin's quantity. Fundamental considerations and operational advantages of such interference were introduced as motivation of this thesis.

We described the theory for an atomic equivalent of optical triple-slit experiment, which opens up possibility of improving the bound of third order interference κ to 10^{-5} as compared to state-of-the-art optical experiments which measured 10^{-4}.

We exploited various methods such as non-linear optics or non-linear Schrödinger equation to achieve non-zero Sorkin's quantity in otherwise canonical quantum mechanics. They give insights on how much non-linearity is present in the setup when an experiment gives non-zero Sorkin's quantity, which allows experimentalists to make accurate measurements and make calibrations of apparatus.

We finally went one step further and described a "post-quantum" theory of density cubes, a model which naturally encompasses multi-path coherence. We showed that the model has operational advantage in the "Elitzur-Vaidman bomb test" as compared to standard quantum mechanics. However, the advantage is considered too strong and trivializes position measurement, and therefore we propose that this feature should not exist in nature.

Appendices

Appendix A

Interference of indistinguishable particles

A.1 Optimal setup for three-path optical experiment

The design in Fig. 3.2 is not the only possible setup to produce non-zero $\mathcal{S}^3$. However, in this appendix we show that for simple combinations of non-linear elements and beam-splitters, our choice is optimal.

First we replace the beam-splitter in Fig. 3.2 with non-linear element. At first glance, this satisfies the "non-linearity in all paths" requirement. However we show that it is actually not true.
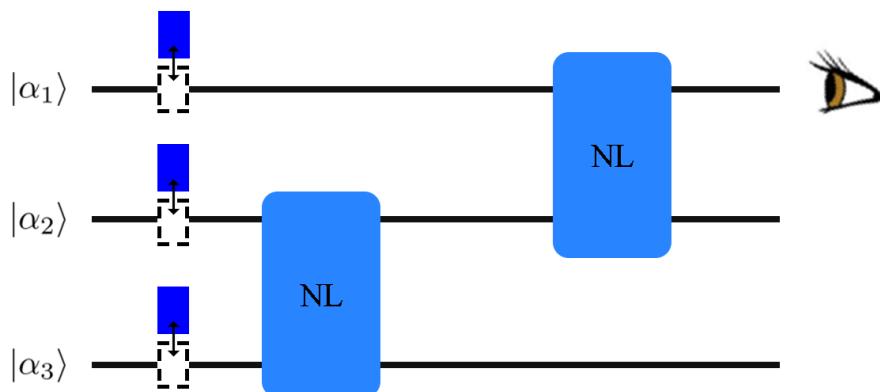
Figure A.1: Alternate design of three-path optical experiment. The beam-splitter in Fig. 3.2 is replaced with a second non-linear element U_{12}.

The corresponding Sorkin's quantity is:

$$
\begin{aligned}
\mathcal{S}^3 &= \text{Tr}(U_{23}^\dagger U_{12}^\dagger a_1^\dagger a_1 U_{12} U_{23} \hat{I}^3) \\
&= \text{Tr}(U_{23}^\dagger a_1^\dagger e^{-i\theta N_2} e^{i\theta N_2} a_1 U_{23} \hat{I}^3)
\end{aligned}
$$

which immediately tells us that the non-linearity in path 2 is cancelled out.

$$
\begin{aligned}
&= \text{Tr}(a_1^\dagger a_1 \hat{I}^3) \\
&= 0
\end{aligned}
\tag{A.1}
$$

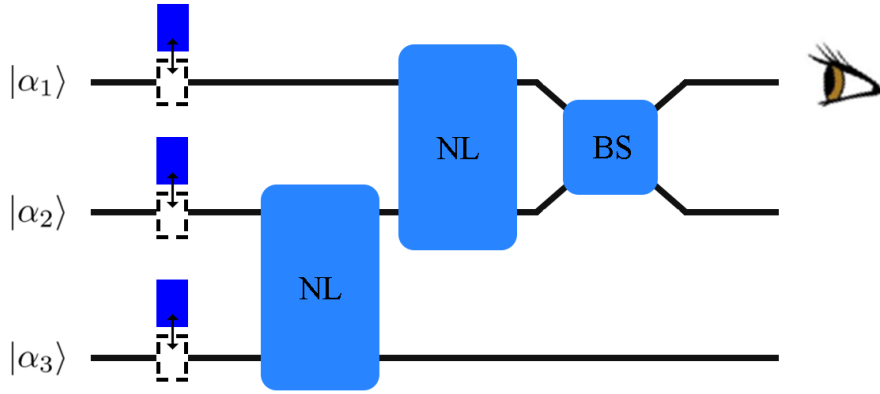Next design is a combination of Fig. 3.2 and Fig. A.1, with two non-linear elements and a beam-splitter.

Figure A.2: Alternate design of three-path optical experiment. It contains two non-linear elements U_{23} and U_{12}, and a beam-splitter S_{12}, followed by the usual intensity measurement in path 1.

Again, we calculate the corresponding $\mathcal{S}^3$:

$$
\begin{aligned}
\mathcal{S}^3 =& \mathrm{Tr}(U_{23}^\dagger U_{12}^\dagger S_{12}^\dagger a_1^\dagger a_1 S_{12} U_{12} U_{23} \hat{I}^3) \\
=& \frac{1}{2} \mathrm{Tr}(U_{23}^\dagger U_{12}^\dagger (a_1^\dagger a_1 + a_1^\dagger a_2 + a_2^\dagger a_1 + a_2^\dagger a_2) U_{12} U_{23} \hat{I}^3) \\
=& \frac{1}{2} \mathrm{Tr}[(a_1^\dagger a_1 + a_2^\dagger a_2 + U_{23}^\dagger e^{-i\theta N_2} a_1^\dagger a_2 e^{i\theta N_1} U_{23} + U_{23}^\dagger e^{-i\theta N_1} a_2^\dagger a_1 e^{i\theta N_2} U_{23}) \hat{I}^3] \\
=& \frac{1}{2} \langle \alpha_1 | a_1^\dagger e^{i\theta N_1} | \alpha_1 \rangle \, (\langle \alpha_2 \alpha_3 | U_{23}^\dagger e^{-i\theta N_2} U_{23} U_{23}^\dagger a_2 U_{23} | \alpha_2 \alpha_3 \rangle \\
& - \langle \alpha_2 0_3 | U_{23}^\dagger e^{-i\theta N_2} U_{23} U_{23}^\dagger a_2 U_{23} | \alpha_2 0_3 \rangle) + h.c. \qquad \text{(A.2a)} \\
=& \frac{1}{2} \alpha_1^* [\langle \alpha_1 | e^{i\theta} \alpha_1 \rangle \langle \alpha_2 \alpha_3 | U_{23}^\dagger e^{-i\theta N_2} U_{23} a_2 e^{i\theta N_3} | \alpha_2 \alpha_3 \rangle \\
& - \langle \alpha_2 0_3 | U_{23}^\dagger e^{-i\theta N_2} U_{23} a_2 e^{i\theta N_3} | \alpha_2 0_3 \rangle] + h.c. \\
=& \frac{1}{2} [\alpha_1^* \alpha_2 \langle \alpha_1 | e^{i\theta} \alpha_1 \rangle \langle \alpha_2 | e^{-i\theta} \alpha_2 \rangle \, (\langle \alpha_3 | e^{i\theta} \alpha_3 \rangle - 1) \\
& + \alpha_1 \alpha_2^* \langle \alpha_1 | e^{-i\theta} \alpha_1 \rangle \langle \alpha_2 | e^{i\theta} \alpha_2 \rangle \, (\langle \alpha_3 | e^{-i\theta} \alpha_3 \rangle - 1)] \qquad \text{(A.2b)}
\end{aligned}
$$

where we inserted $U_{23} U_{23}^\dagger = \mathbb{1}$ in step A.2a and used the cyclic property of trace in the last step. When we compare the result to Eq. 3.12, the extra terms in A.2b are all less than 1.

$$
\langle \alpha_1 | e^{i\theta} \alpha_1 \rangle < 1 \qquad \text{(A.3a)}
$$
$$
\langle \alpha_2 | e^{-i\theta} \alpha_2 \rangle < 1 \qquad \text{(A.3b)}
$$

This means the setup in Fig. A.2 has less non-linearity as compared to the one in Fig. 3.2, which makes detection more difficult. At the same time, it has more elements which increased the possibility of experimental errors.
Similarly, we derive $\mathcal{S}^3$ for other setups containing two non-linear elements and a beam-splitter.
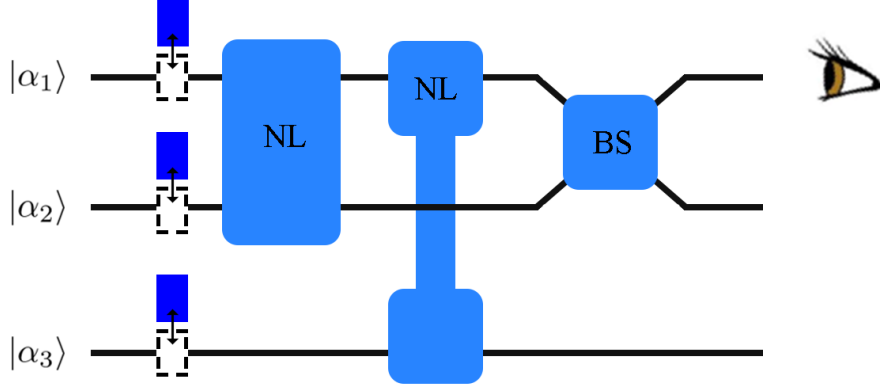
Figure A.3: Setup containing two non-linear elements U_{12} and U_{13}, and a beam-splitter S_{12}, followed by intensity measurement in path 1.

$$
\begin{aligned}
\mathcal{S}^3 =& \mathrm{Tr}(U_{12}^\dagger U_{13}^\dagger S_{12}^\dagger a_1^\dagger a_1 S_{12} U_{13} U_{12} \hat{I}^3) \\
=& \frac{1}{2} \mathrm{Tr}(U_{12}^\dagger U_{13}^\dagger (a_1^\dagger a_1 + a_1^\dagger a_2 + a_2^\dagger a_1 + a_2^\dagger a_2) U_{13} U_{12} \hat{I}^3) \\
=& \frac{1}{2} \mathrm{Tr}[(a_1^\dagger a_1 + a_2^\dagger a_2 + U_{12}^\dagger e^{-i\theta N_3} a_1^\dagger a_2 U_{12} + U_{12}^\dagger a_2^\dagger a_1 e^{i\theta N_3} U_{12}) \hat{I}^3] \\
=& \frac{1}{2} \langle \alpha_1 | a_1^\dagger e^{i\theta N_1} | \alpha_1 \rangle \langle \alpha_2 | e^{-i\theta N_2} a_2 | \alpha_2 \rangle (\langle \alpha_3 | e^{-i\theta N_3} | \alpha_3 \rangle - 1) + h.c. \\
=& \frac{1}{2} [\alpha_1^* \alpha_2 \langle \alpha_1 | e^{i\theta} \alpha_1 \rangle \langle \alpha_2 | e^{-i\theta} \alpha_2 \rangle (\langle \alpha_3 | e^{-i\theta} \alpha_3 \rangle - 1) \\
& + \alpha_1 \alpha_2^* \langle \alpha_1 | e^{-i\theta} \alpha_1 \rangle \langle \alpha_2 | e^{i\theta} \alpha_2 \rangle (\langle \alpha_3 | e^{i\theta} \alpha_3 \rangle - 1)]
\end{aligned}
\tag{A.4}
$$

Again we reached the same conclusion as above. This setup is both less effective and more prone to error.

Finally, for completeness sake, we calculate the setup which has non-linear elements U_{23} and U_{13}
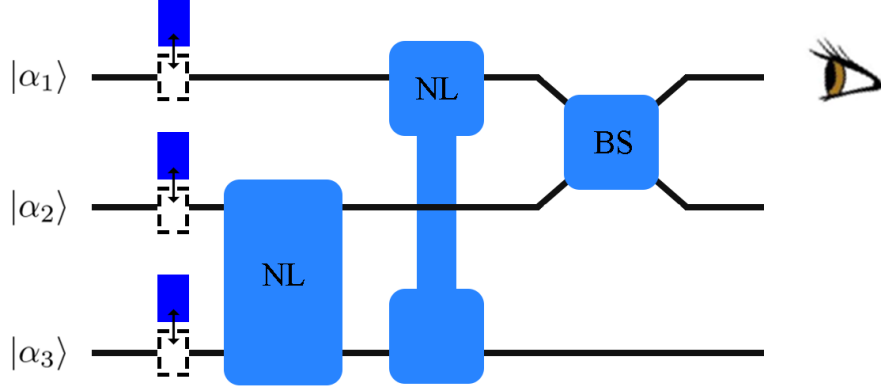
Figure A.4: The final combination of two non-linear elements three-path optical experiment. It contains U_{23} and U_{13}, and a beam-splitter S_{12}, followed by intensity measurement in path 1.

$$
\begin{aligned}
\mathcal{S}^3 =& \mathrm{Tr}(U_{23}^\dagger U_{13}^\dagger S_{12}^\dagger a_1^\dagger a_1 S_{12} U_{13} U_{23} \hat{I}^3) \\
=& \frac{1}{2}\mathrm{Tr}[(a_1^\dagger a_1 + a_2^\dagger a_2 + U_{23}^\dagger e^{-i\theta N_3} a_1^\dagger a_2 U_{23} + U_{23}^\dagger a_2^\dagger a_1 e^{i\theta N_3} U_{23})\hat{I}^3] \\
=& 0 \tag{A.5}
\end{aligned}
$$

due to the absence of non-linearity in path 1.

We have derived $\mathcal{S}^3$ for single-, double-, and triple-non-linear elements setups, and found the optimal solution to be the single-element setup in the main text.

Appendix B

Density cube model

B.1 Solution to the orthonormality equations for optimal cubes

The solution is divided into two parts: N even and N odd. The aim is to find vectors $\vec{x}_m, \vec{x}_n$ which satisfy the relation $(\vec{x}_m, \vec{x}_n) + (\vec{x}_n, \vec{x}_m) = 2 - N$.

B.1.1 N even

Let M be a $(N-1) \times N$ matrix formed from the discrete $N \times N$ Fourier transform by deleting the first row:

$$
M = \begin{pmatrix}
1 & \omega^{1 \cdot 1} & \omega^{1 \cdot 2} & \cdots & \omega^{1 \cdot (N-1)} \\
1 & \omega^{2 \cdot 1} & \omega^{2 \cdot 2} & \cdots & \omega^{2 \cdot (N-1)} \\
\vdots & \vdots & \vdots & \ddots & \vdots \\
1 & \omega^{(N-1) \cdot 1} & \omega^{(N-1) \cdot 2} & \cdots & \omega^{(N-1) \cdot (N-1)}
\end{pmatrix}, \qquad \text{(B.1)}
$$

where $\omega = \exp(i2\pi/N)$. The crucial property we shall use is expressed in the following multiplication:

$$
M^\dagger M = \begin{pmatrix}
N-1 & -1 & \cdots & -1 \\
-1 & N-1 & \cdots & -1 \\
\vdots & \vdots & \ddots & \vdots \\
-1 & -1 & \cdots & N-1
\end{pmatrix}. \qquad \text{(B.2)}
$$

Hence, the columns of matrix M form vectors with fixed overlap equal to -1, for any pair of distinct vectors. Let us now form matrix X by stacking

$(N-2)/2$ matrices M vertically:

$$X = \begin{pmatrix} M \\ M \\ \vdots \\ M \end{pmatrix}. \tag{B.3}$$

Note that matrix X has N columns and $(N-1)(N-2)/2$ rows. We therefore define vectors $\vec{x}_n$ as columns of X:

$$X = \begin{pmatrix} \vec{x}_1 & \vec{x}_2 & \cdots & \vec{x}_N \end{pmatrix}. \tag{B.4}$$

Now, $\vec{x}_n$ satisfy our requirement:

$$(\vec{x}_m, \vec{x}_n) + (\vec{x}_n, \vec{x}_m) = 2(\vec{x}_m, \vec{x}_n) = (N-2)(M^\dagger M)_{mn} \quad \text{for m} \neq \text{n}$$
$$= 2 \cdot \frac{N-2}{2} \cdot (-1) = 2 - N. \tag{B.5}$$

B.1.2 N odd

Now we construct matrix M, having dimensions $\frac{N-1}{2} \times N$, by deleting the first row of the $N \times N$ Fourier transform matrix and taking only $\frac{N-1}{2}$ top rows left:

$$M = \begin{pmatrix} 1 & \omega^{1\cdot 1} & \omega^{1\cdot 2} & \cdots & \omega^{1\cdot N} \\ 1 & \omega^{1\cdot 1} & \omega^{1\cdot 2} & \cdots & \omega^{1\cdot N} \\ \vdots & \vdots & \vdots & \ddots & \vdots \\ 1 & \omega^{\frac{N-1}{2}\cdot 1} & \omega^{\frac{N-1}{2}\cdot 2} & \cdots & \omega^{\frac{N-1}{2}\cdot N} \end{pmatrix}. \tag{B.6}$$

This time we have:

$$M^\dagger M = \begin{pmatrix} \frac{N-1}{2} & -\frac{1}{2} & \cdots & -\frac{1}{2} \\ -\frac{1}{2} & \frac{N-1}{2} & \cdots & -\frac{1}{2} \\ \vdots & \vdots & \ddots & \vdots \\ -\frac{1}{2} & -\frac{1}{2} & \cdots & \frac{N-1}{2} \end{pmatrix} + i \,(\text{imaginary part}). \tag{B.7}$$

We form matrix X by stacking $N-2$ matrices M vertically and define vectors $\vec{x}_n$ as columns of X as before. Indeed the overlap between distinct vectors reads:

$$\begin{aligned} (\vec{x}_m, \vec{x}_n) + (\vec{x}_n, \vec{x}_m) &= 2\text{Re}\left[(\vec{x}_m, \vec{x}_n)\right] \\ &= 2\text{Re}(X^\dagger X)_{mn} & \text{for m} \neq \text{n} \\ &= 2(N-2)\text{Re}(M^\dagger M)_{mn} & \text{for m} \neq \text{n} \\ &= 2 - N. \end{aligned} \tag{B.8}$$

B.2 Example of resulting cubes for $N = 4$

The following four cubes are obtained for the four-path interferometer.

$$\frac{1}{3\sqrt{3}}\left\{\begin{pmatrix} 0 & 0 & 0 & 0 \\ 0 & 0 & 1 & 1 \\ 0 & 1 & 0 & 1 \\ 0 & 1 & 1 & 0 \end{pmatrix}, \begin{pmatrix} 0 & 0 & 1 & 1 \\ 0 & \sqrt{3} & 0 & 0 \\ 1 & 0 & 0 & 0 \\ 1 & 0 & 0 & 0 \end{pmatrix}, \begin{pmatrix} 0 & 1 & 0 & 1 \\ 1 & 0 & 0 & 0 \\ 0 & 0 & \sqrt{3} & 0 \\ 1 & 0 & 0 & 0 \end{pmatrix}, \begin{pmatrix} 0 & 1 & 1 & 0 \\ 1 & 0 & 0 & 0 \\ 1 & 0 & 0 & 0 \\ 0 & 0 & 0 & \sqrt{3} \end{pmatrix}\right\},$$

$$\frac{1}{3\sqrt{3}}\left\{\begin{pmatrix} \sqrt{3} & 0 & 0 & 0 \\ 0 & 0 & -i & -1 \\ 0 & i & 0 & i \\ 0 & -1 & -i & 0 \end{pmatrix}, \begin{pmatrix} 0 & 0 & i & -1 \\ 0 & 0 & 0 & 0 \\ -i & 0 & 0 & 0 \\ -1 & 0 & 0 & 0 \end{pmatrix}, \begin{pmatrix} 0 & -i & 0 & i \\ i & 0 & 0 & 0 \\ 0 & 0 & \sqrt{3} & 0 \\ -i & 0 & 0 & 0 \end{pmatrix}, \begin{pmatrix} 0 & -1 & -i & 0 \\ -1 & 0 & 0 & 0 \\ i & 0 & 0 & 0 \\ 0 & 0 & 0 & \sqrt{3} \end{pmatrix}\right\},$$

$$\frac{1}{3\sqrt{3}}\left\{\begin{pmatrix} \sqrt{3} & 0 & 0 & 0 \\ 0 & 0 & -1 & 1 \\ 0 & -1 & 0 & -1 \\ 0 & 1 & -1 & 0 \end{pmatrix}, \begin{pmatrix} 0 & 0 & -1 & 1 \\ 0 & \sqrt{3} & 0 & 0 \\ -1 & 0 & 0 & 0 \\ 1 & 0 & 0 & 0 \end{pmatrix}, \begin{pmatrix} 0 & -1 & 0 & -1 \\ -1 & 0 & 0 & 0 \\ 0 & 0 & 0 & 0 \\ -1 & 0 & 0 & 0 \end{pmatrix}, \begin{pmatrix} 0 & 1 & -1 & 0 \\ 1 & 0 & 0 & 0 \\ -1 & 0 & 0 & 0 \\ 0 & 0 & 0 & \sqrt{3} \end{pmatrix}\right\},$$

$$\frac{1}{3\sqrt{3}}\left\{\begin{pmatrix} \sqrt{3} & 0 & 0 & 0 \\ 0 & 0 & i & -1 \\ 0 & -i & 0 & -i \\ 0 & -1 & i & 0 \end{pmatrix}, \begin{pmatrix} 0 & 0 & -i & -1 \\ 0 & \sqrt{3} & 0 & 0 \\ i & 0 & 0 & 0 \\ -1 & 0 & 0 & 0 \end{pmatrix}, \begin{pmatrix} 0 & i & 0 & -i \\ -i & 0 & 0 & 0 \\ 0 & 0 & \sqrt{3} & 0 \\ i & 0 & 0 & 0 \end{pmatrix}, \begin{pmatrix} 0 & -1 & i & 0 \\ -1 & 0 & 0 & 0 \\ -i & 0 & 0 & 0 \\ 0 & 0 & 0 & 0 \end{pmatrix}\right\}.$$

Other solutions for four-path interferometer are possible in Subsec. B.3.2.

B.3 Consistency of the transformation

B.3.1 Positivity of matrix D

We shall find the eigenvalues of $\mathbb{1} - BB^\dagger$ explicitly. Since $B = (X \; X^*)^t$, where t denotes transpose, the construction in B.1 for even N gives

$$BB^\dagger = \frac{1}{(N-1)^2}\left(\begin{array}{ccc|ccc} MM^\dagger & \cdots & MM^\dagger & M^*M^\dagger & \cdots & M^*M^\dagger \\ \vdots & \ddots & \vdots & \vdots & \ddots & \vdots \\ MM^\dagger & \cdots & MM^\dagger & M^*M^\dagger & \cdots & M^*M^\dagger \\ \hline MM^t & \cdots & MM^t & M^*M^t & \cdots & M^*M^t \\ \vdots & \ddots & \vdots & \vdots & \ddots & \vdots \\ MM^t & \cdots & MM^t & M^*M^t & \cdots & M^*M^t \end{array}\right),$$

(B.9)

Note that $MM^\dagger = N\mathbb{1}$ inherited from the unitarity of the Fourier matrix. Similarly $M^*M^t = (M^\dagger)^t M^t = (MM^\dagger)^t = N\mathbb{1}$. Direct computation shows

$MM^t = M^*M^\dagger = N\,\mathbb{1}^A$, where $\mathbb{1}^A$ denotes an anti-diagonal matrix with all non-zero elements being 1. Therefore, matrix $(N-1)^2 BB^\dagger$ has the following form for even N:

$$
\left(
\begin{array}{cccc|cccc}
1 & & 1 & & & 1 & & 1 \\
& \ddots & \cdots & \ddots & & \cdot^{\cdot^\cdot} & \cdots & \cdot^{\cdot^\cdot} \\
& 1 & & 1 & 1 & & 1 & \\
\vdots & & \vdots & & & \vdots & & \vdots \\
1 & & 1 & & & 1 & & 1 \\
& \ddots & \cdots & \ddots & & \cdot^{\cdot^\cdot} & \cdots & \cdot^{\cdot^\cdot} \\
& 1 & & 1 & 1 & & 1 & \\
\hline
& 1 & & 1 & 1 & & 1 & \\
\cdot^{\cdot^\cdot} & & \cdots & \cdot^{\cdot^\cdot} & & \ddots & \cdots & \ddots \\
1 & & 1 & & & 1 & & 1 \\
\vdots & & \vdots & & & \vdots & & \vdots \\
& 1 & & 1 & 1 & & 1 & \\
\cdot^{\cdot^\cdot} & & \cdots & \cdot^{\cdot^\cdot} & & \ddots & \cdots & \ddots \\
1 & & 1 & & & 1 & & 1
\end{array}
\right) . \qquad \text{(B.10)}
$$

Similarly one finds for odd N:

$$
\left(
\begin{array}{cccc|cccc}
1 & & 1 & & & & & \\
& \ddots & \cdots & \ddots & & & & \\
& 1 & & 1 & & & & \\
\vdots & & \vdots & & & & 0 & \\
1 & & 1 & & & & & \\
& \ddots & \cdots & \ddots & & & & \\
& 1 & & 1 & & & & \\
\hline
& & & & 1 & & 1 & \\
& & & & & \ddots & \cdots & \ddots \\
& & & & & 1 & & 1 \\
& & 0 & & \vdots & & \vdots & \\
& & & & 1 & & 1 & \\
& & & & & \ddots & \cdots & \ddots \\
& & & & & 1 & & 1
\end{array}
\right) . \qquad \text{(B.11)}
$$

In both cases of N being even or odd, the eigenvalues of $BB^\dagger$ are either 0 or $N(N-2)/(N-1)^2$. Hence the eigenvalues of D^2 are either 1 or $1/(N-1)^2$.

B.3.2 Exemplary transformation for $N = 4$

We shall only present the D matrices. Following the method above one can find the principle square root as:

$$D = \frac{1}{3} \begin{pmatrix} 2 & 0 & 0 & 0 & 0 & -1 \\ 0 & 2 & 0 & 0 & -1 & 0 \\ 0 & 0 & 2 & -1 & 0 & 0 \\ 0 & 0 & -1 & 2 & 0 & 0 \\ 0 & -1 & 0 & 0 & 2 & 0 \\ -1 & 0 & 0 & 0 & 0 & 2 \end{pmatrix}. \tag{B.12}$$

This is not the only solution given the constraints of $\mathcal{T}^2 = \mathbb{1}$ and $\mathcal{T} = \mathcal{T}^\dagger$. Other solutions are possible with eigenvalues ± 1 or $\pm 1/(N-1)$, since we are only interested in eigenvalues of D^2 for the positivity condition. The following two matrices were obtained by other means:

$$D_2 = \frac{1}{3} \begin{pmatrix} 1 & -i & i & -i & i & 0 \\ i & 1 & 1 & -1 & 0 & -i \\ -i & 1 & 1 & 0 & -1 & i \\ i & -1 & 0 & 1 & 1 & -i \\ -i & 0 & -1 & 1 & 1 & i \\ 0 & i & -i & i & -i & 1 \end{pmatrix}, \tag{B.13}$$

$$D_3 = \frac{1}{3} \begin{pmatrix} 1 & -1 & -i & i & 1 & 0 \\ -1 & 1 & -i & i & 0 & 1 \\ i & i & 1 & 0 & -i & -i \\ -i & -i & 0 & 1 & i & i \\ 1 & 0 & i & -i & 1 & -1 \\ 0 & 1 & i & -i & -1 & 1 \end{pmatrix}. \tag{B.14}$$

If we use D_3 as an example, then $\mathcal{T}$ has the following elements:

$$\mathcal{T} = \frac{1}{3} \begin{pmatrix} 0 & 1 & 1 & 1 & 1 & 1 & 1 & 1 & 1 & 1 \\ 1 & 0 & 1 & 1 & i & -1 & -i & -i & -1 & i \\ 1 & 1 & 0 & 1 & -1 & 1 & -1 & -1 & 1 & -1 \\ 1 & 1 & 1 & 0 & -i & -1 & i & i & -1 & -i \\ 1 & -i & -1 & i & 1 & -1 & -i & i & 1 & 0 \\ 1 & -1 & 1 & -1 & -1 & 1 & -i & i & 0 & 1 \\ 1 & i & -1 & -i & i & i & 1 & 0 & -i & -i \\ 1 & i & -1 & -i & -i & -i & 0 & 1 & i & i \\ 1 & -1 & 1 & -1 & 1 & 0 & i & -i & 1 & -1 \\ 1 & -i & -1 & i & 0 & 1 & i & -i & -1 & 1 \end{pmatrix}. \tag{B.15}$$

Bibliography

[1] The original double slit experiment. *Online, v=Iuv6hY6zsd0*, 2013.

[2] O. Donati, G. P. Missiroli, and G. Pozzi. An experiment on electron interference. *Am. J. Phys.*, 41(5):639–644, 1973.

[3] O. Nairz, B. Brezger, M. Arndt, and A. Zeilinger. Diffraction of complex molecules by structures made of light. *Phys. Rev. Lett.*, 87:160401, Sep 2001.

[4] O. Nairz, M. Arndt, and A. Zeilinger. Quantum interference experiments with large molecules. *Am. J. Phys.*, 71(4):319–325, 2003.

[5] S. Eibenberger, S. Gerlich, M. Arndt, M. Mayor, and J. Tüxen. Matter-wave interference of particles selected from a molecular library with masses exceeding 10 000 amu. *Phys. Chem. Chem. Phys.*, 15:14696–14700, 2013.

[6] R. S. Aspden, M. J. Padgett, and G. C. Spalding. Video recording true single-photon double-slit interference. *Am. J. Phys.*, 84(9):671–677, 2016.

[7] R. D. Sorkin. Quantum mechanics as quantum measure theory. *Mod. Phys. Lett. A 9, 3119–3128.*, 1994.

[8] U. Sinha, C. Couteau, T. Jennewein, R. Laflamme, and G. Weihs. Ruling out multi-order interference in quantum mechanics. *Science*, 329(5990):418–421, 2010.

[9] I. Söllner, B. Gschösser, P. Mai, B. Pressl, Z. Vörös, and G. Weihs. Testing born's rule in quantum mechanics for three mutually exclusive events. *Found. Phys*, 42(6):742–751, Jun 2012.

[10] D. K. Park, O. Moussa, and R. Laflamme. Three path interference using nuclear magnetic resonance: a test of the consistency of born's rule. *New J. Phys.*, 14(11):113025, Nov 2012.

[11] T. Kauten, R. Keil, T. Kaufmann, B. Pressl, Č. Brukner, and G. Weihs. Obtaining tight bounds on higher-order interferences with a 5-path interferometer. *New J. Phys.*, 19(3):033017, Mar 2017.

[12] O. S. Magaña-Loaiza, I. De Leon, M. Mirhosseini, R. Fickler, A. Safari, U. Mick, B. McIntyre, P. Banzer, B. Rodenburg, G. Leuchs, and R. W. Boyd. Exotic looped trajectories of photons in three-slit interference. *Nat. Commun.*, 7(1):13987, 2016.

[13] C. M. Lee and J. H. Selby. Higher-order interference in extensions of quantum theory. *Found. Phys.*, 47:89–112, 2017.

[14] C. M. Lee and J. H. Selby. Generalised phase kick-back: the structure of computational algorithms from physical principles. *New J. Phys.*, 18(3):033023, mar 2016.

[15] C. M. Lee and J. H. Selby. Deriving grover's lower bound from simple physical principles. *New J. Phys.*, 18(9):093047, sep 2016.

[16] H. Yabuki. Feynman path integrals in the Young double-slit experiment. *International Journal of Theoretical Physics*, 25(2):159–174, Feb 1986.

[17] H. De Raedt, K. Michielsen, and K. Hess. Analysis of multipath interference in three-slit experiments. *Phys. Rev. A*, 85:012101, Jan 2012.

[18] R. Sawant, J. Samuel, A. Sinha, S. Sinha, and U. Sinha. Nonclassical paths in quantum interference experiments. *Phys. Rev. Lett.*, 113:120406, Sep 2014.

[19] A. Sinha, A. H. Vijay, and U. Sinha. On the superposition principle in interference experiments. *Sci. Rep.*, 5(1):10304, 2015.

[20] G. Rengaraj, U. Prathwiraj, S. N. Sahoo, R Somashekhar, and U. Sinha. Measuring the deviation from the superposition principle in interference experiments. *New J. Phys.*, 20(6):063049, jun 2018.

[21] T. Xin, L. Hao, S-Y. Hou, G-R. Feng, and G-L. Long. Preparation of pseudo-pure states for NMR quantum computing with one ancillary qubit. *Sci. China Phys. Mech.*, 62(6):960312, Mar 2019.

[22] R. Das, A. Mitra, S. V. Kumar, and A. Kumar. Quantum information processing by NMR: Preparation of pseudopure states and implementation of unitary operations in a single-qutrit system. *Int. J. Quantum Inf.*, 01(03):387–394, 2003.

[23] F. Leroux, K. Pandey, R. Rehbi, F. Chevy, C. Miniatura, B. Grémaud, and D. Wilkowski. Non-Abelian adiabatic geometric transformations in a cold strontium gas. *Nat. Commun.*, 9(1):3580, 2018.

[24] M. Żukowski, A. Zeilinger, and M. A. Horne. Realizable higher-dimensional two-particle entanglements via multiport beam splitters. *Phys. Rev. A*, 55:2564–2579, Apr 1997.

[25] A. J. Leggett. Experimental approaches to the quantum measurement paradox. *Found. Phys*, 18(9):939–952, Sep 1988.

[26] N. V. Vitanov, A. A. Rangelov, B. W. Shore, and K. Bergmann. Stimulated Raman adiabatic passage in physics, chemistry, and beyond. *Rev. Mod. Phys.*, 89:015006, Mar 2017.

[27] W. Bao, D. Jaksch, and P. A. Markowich. Numerical solution of the Gross–Pitaevskii equation for Bose–Einstein condensation. *J. Comput. Phys.*, 187(1):318 – 342, 2003.

[28] C. Huepe, S. Métens, G. Dewel, P. Borckmans, and M. E. Brachet. Decay rates in attractive Bose-Einstein condensates. *Phys. Rev. Lett.*, 82:1616–1619, Feb 1999.

[29] J Rogel-Salazar. The Gross–Pitaevskii equation and Bose–Einstein condensates. *Eur. J. Phys.*, 34(2):247–257, Jan 2013.

[30] M. K. Akhlaghi, A. H. Majedi, and J. S. Lundeen. Nonlinearity in single photon detection: modeling and quantum tomography. *Opt. Express*, 19(22):21305–21312, Oct 2011.

[31] H-Y. Lo, Y-C. Chen, P-C. Su, H-C. Chen, J-X. Chen, Y-C. Chen, I. A. Yu, and Y-F. Chen. Electromagnetically-induced-transparency-based cross-phase-modulation at attojoule levels. *Phys. Rev. A*, 83:041804, Apr 2011.

[32] B-W. Shiau, M-C. Wu, C-C. Lin, and Y-C. Chen. Low-light-level cross-phase modulation with double slow light pulses. *Phys. Rev. Lett.*, 106:193006, May 2011.

[33] T. Kauten, B. Pressl, T. Kaufmann, and G. Weihs. Measurement and modeling of the nonlinearity of photovoltaic and Geiger-mode photodiodes. *Rev. Sci. Instrum.*, 85(6):063102, 2014.

[34] J. Söding, D. Guéry-Odelin, P. Desbiolles, F. Chevy, H. Inamori, and J. Dalibard. Three-body decay of a Rubidium Bose–Einstein condensate. *Appl. Phys. B*, 69(4):257–261, Oct 1999.

[35] A. C. Elitzur and L. Vaidman. Quantum mechanical interaction-free measurements. *Found. Phys.*, 23(7):987–997, 1993.

[36] L. Vaidman. On the realisation of interaction-free measurements. *Quant. Opt.*, 6:119–126, 1994.

[37] P. Kwiat, H. Weinfurter, T. Herzog, A. Zeilinger, and M. A. Kasevich. Interaction-free measurement. *Phys. Rev. Lett.*, 74:4763, 1995.

[38] M. Hafner and J. Summhammer. Experiment on interaction-free measurement in neutron interferometry. *Phys. Lett. A*, 235(6):563 – 568, 1997.

[39] T. Tsegaye, E. Goobar, A. Karlsson, G. Björk, M. Y. Loh, and K. H. Lim. Efficient interaction-free measurements in a high-finesse interferometer. *Phys. Rev. A*, 57:3987–3990, May 1998.

[40] C. Robens, W. Alt, C. Emary, D. Meschede, and A. Alberti. Atomic "bomb testing": the Elitzur–Vaidman experiment violates the Leggett–Garg inequality. *Appl. Phys. B*, 123:12, 2017.

[41] G. S. Paraoanu. Interaction-free measurements with superconducting qubits. *Phys. Rev. Lett.*, 97:180406, Nov 2006.

[42] W. K. Wootters and W. H. Zurek. A single quantum cannot be cloned. *Nature*, 299:802 – 803, 1982.

[43] D. Dieks. Communication by EPR devices. *Phys. Lett. A*, 92:271 – 272, 1982.

[44] H. Barnum, C. M. Caves, C. A. Fuchs, R. Jozsa, and B. Schumacher. Noncommuting mixed states cannot be broadcast. *Phys. Rev. Lett.*, 76:2818, 1996.

[45] M. Piani, P. Horodecki, and R. Horodecki. No-local-broadcasting theorem for multipartite quantum correlations. *Phys. Rev. Lett.*, 100:090502, 2008.

[46] A. K. Pati and S. L. Braunstein. Impossibility of deleting an unknown quantum state. *Nature*, 404:164 – 165, 2000.

[47] B Dakić, T Paterek, and Č Brukner. Density cubes and higher-order interference theories. *New J. Phys.*, 16(2):023028, feb 2014.

[48] Y. Tikochinsky. Feynman rules for probability amplitudes. *Int. J. Theor. Phys.*, 27:543, 1988.

[49] P. Goyal, K. H. Knuth, and J. Skilling. Origin of complex quantum amplitudes and Feynman's rules. *Phys. Rev. A*, 81:022109, 2010.

[50] A. J. Short and J. Barrett. Strong nonlocality: a trade-off between states and measurements. *New J. Phys.*, 12(3):033034, mar 2010.

[51] A. Wilce. Symmetry, self-duality and the Jordan structure of quantum mechanics. *arXiv:1110.6607*, 2011.

[52] S. Popescu and D. Rohrlich. Quantum nonlocality as an axiom. *Found. Phys.*, 24:379 – 385, 1994.

[53] W. van Dam. *Nonlocality and Communication Complexity.* PhD thesis, University of Oxford, 2000.

[54] G. Brassard, H. Buhrman, N. Linden, A. A. Methot, A. Tapp, and F. Unger. Limit on nonlocality in any world in which communication complexity is not trivial. *Phys. Rev. Lett.*, 96:250401, 2006.

[55] M. Pawłowski, T. Paterek, D. Kaszlikowski, V. Scarani, A. Winter, and M. Żukowski. Information causality as a physical principle. *Nature*, 461:1101 – 1104, 2009.

[56] M. Navascues and H. Wunderlich. A glance beyond the quantum model. *Proc. Roy. Soc. A*, 466:881 – 890, 2010.

[57] O. C. O. Dahlsten, D. Lercher, and R. Renner. Tsirelson's bound from a generalised data processing inequality. *New J. Phys.*, 14:063024, 2012.